

# Iterative data enhancement of ambient vibration tests for the Nitrate-prilling tower in Shiraz petrochemical complex

Emad Ahangar Ebrahimi<sup>1</sup>, Hassan Yousefi<sup>1,\*</sup>, Iradj Mahmoudzadeh Kani<sup>1</sup>, Alireza Taghavi Kani<sup>1</sup>

<sup>1</sup>School of Civil Engineering, College of Engineering, University of Tehran, Tehran, Iran.

\*Corresponding author: Email: [hyosefi@ut.ac.ir](mailto:hyosefi@ut.ac.ir)

## Abstract

In this study, the discrete wavelet packet transform (DWPT) has been used for the single-step and iterative denoising methods for enhancing data with high level of noise to identification of modal frequencies in ambient vibration tests on a petrochemical process tower in Shiraz, Iran. The ambient vibration test is performed by the wind load. All mechanical systems operated during the test; hence, different noise sources exist. Here, both high and low frequency ranges are decomposed effectively in the DWPT, and it provides a lot of global and localized information. The DWPT-based one-step denoising method fails to properly denoise the high-level noisy data with denoising-thresholds obtained by different theoretical methods. For this reason, the so-called peeling approach achieved by an iterative denoising method is used to enhance the quality of the signal. For this iterative method, the parameters are obtained by the trial-and-error method. After the signal-enhancement stage, the signal processing step is performed by continuous wavelet transforms (CWTs) to detect the time-frequency information in the data. Furthermore, the modal frequencies are directly identified by the cross wavelet transform (XWT) and the corresponding spectral power density. Finally, the estimated frequencies by XWT are compared with the natural frequencies of a damaged model simulated by the finite element (FE) method.

**Key words:** Ambient vibration test; Wavelet packet transform; Iterative denoising; Multiresolution analysis; Modal frequencies.

## 1. Introduction

Ambient vibration tests are quick and cheap; they do not require excitation equipment and the source of excitation is environmental loads, such as: wind [1-5], traffic loads [6] and small to moderate earthquakes [7]. These tests are commonly used to identify modal parameters (i.e.: modal frequencies, damping and

modal shapes), in health monitoring studies [3, 8], assessment of real time qualifications [1-5, 8-15] and vibration controls [16]. Identifying the modal parameters of the system is challenging due to non-stationary responses and the high-level of noise in the recorded nonlinear signals in ambient vibrations. Wavelet transforms [3, 4, 7-12, 15, 17-22] provide the time-frequency information of the data with different resolution accuracies and decomposition levels in a non-parametric approach using only the output data. However, the high-level of noise causes also problems in the performance of this powerful transformation [23]. To reduce such shortcomings, here, the wavelet packet transform would be used.

In this study, the main purpose is to identify physical features from data with a high-level of noise using discrete wavelet packet transform with multi-resolution analysis (MRA) approach. The wavelet packet analysis permits to access effectively the time-frequency localized information of both high and low frequency contents. Which is the shortcoming of the common discrete wavelet transform, that is for high-frequency components, it is not possible to distinguish high frequency contents from each other. Two general data denoising or enhancement approaches can be counted in the MRA framework: (1) One-step denoising [24-29], and (2) Iterative-based enhancement [30-36]. In the first case, in one step of MRA, it is tried to remove noise from data. In the iterative approach, noise is estimated and removed from the data by using several iterative steps of MRA. This approach is useful for data with high-level of noise, where one step denoising methods may not be efficient. In noisy data, it is almost impossible to completely filter out the noise, Hence the iterative denoising method can improve or enhance the quality of denoised data. Iterative denoising schemes were initially proposed by Starck and Bijaoui [36], Coifman and Wickerhauser [30, 31], Hadjilleontiadis et al. [32, 33], and Ranta et al. [34, 35].

The results of the ambient vibration tests (e.g., modal frequencies, modal shapes, and damping) can be very sensitive to noise. Few works studied only noise effects (especially effects of high-level of noise). Hence, one of our main goal is to focus on noise-effect reduction to decline sensitivity of results obtained by ambient vibration tests. Especially in this study, due to high-level of noise, the common denoising methods may not be effective. Hence her iterative denoising is introduced which was used before in some few studies for denoising of noisy sound from recorded sounds from lungs or medical images [30,31,36]. Introducing this powerful tool is one of our purposes of the current study. After data denoising in this study, modal frequencies of enhanced data are captured by common continuous wavelet-based transforms for a real case study.

In the iterative method, the recorded raw (initial) signal is considered completely as noise for the first iteration, and the denoised signal is considered to have zero components. For the next iteration, the noise signal (in the previous iteration) is decomposed into different resolution levels by MRA by the wavelet packet transform. Regarding the decomposition results, at the last resolution level ( $J_{\min}$ ), wavelet coefficients that are large enough are considered as physical phenomenon. These coefficients are separated

from noisy information. These wavelet coefficients are reconstructed by the wavelet packet inverse transform and then are added to previous denoised (detected) information from the previous iteration (for instance, the zero vector at the first iteration). The remaining wavelet coefficients (with small values) are reconstructed as updated noise for use in the next iteration. This iterative procedure is repeated step-by-step until reaching a pre-determined criterion. Because physical information is collected layer by layer from residual noise, this approach is also expressed as “peeling off successive layers” scheme [30, 31]. In this iterative method, in each iteration, it is assumed that the wavelet coefficients with large enough values belong to physical information. These wavelet coefficients are detected based on (predefined) thresholds at the last resolution level in the wavelet-packet transform. These thresholds can be determined by means of the variance of wavelet coefficient values at the last resolution level (for instance see the last row, level 4, in Fig. 1; in this level, for each decomposed set of coefficients, corresponding variance can be calculated. For each set, then, the threshold value would be proportional to corresponding variance). In general, the threshold values can be chosen based on some criteria or even empirically.

By comparing the results of the iterative denoising approach with the results of the one-step denoising approach for data with high-level of noise and so with small signal-noise-ratio (SNR) values (here, in ambient vibration testing), the importance of using the iterative denoising method would be confirmed.

Although the quality of the signals is improved by the iterative algorithm, it is still a difficult and challenging task to determine the physical properties in such improved data.

In this study, the concept of cross wavelet analysis [25, 37] and the corresponding spectral power have been used to improve the ability of detection of physical features. These transformations would be used for denoised data obtained from the iterative denoising algorithm. Cross-wavelet analysis allows the identification of physical features common in two signals with significant common energy in time-frequency space. Since noise has a random property, two recorded data are expected to have different noise energies at different times and resolutions. Hence, noise effects would be diminished in cross analysis.

Also, the spectral power of the cross-wavelet transform can help to identify the locally excited frequencies in the frequency domain. Features that have both time continuity and energy concentration with large values in spectral power representation could include physical phenomena. In identifying the modal frequencies for modes with small contributions, simultaneous investigation can be helpful, (which is later discussed in this study).

At last, it should be noted that the abovementioned signal-enhancement method with iterative denoising concept can be integrated (as a preprocessor) with other wavelet-based methods developed to identify modal parameters, see e.g. [4, 12, 38].

Here, wavelet-based time-frequency representations are used to detect physical features. There are other methods for studying MRA, such as the Hilbert-Huang transform (HHT) [18].

This study is composed of nine parts. Section 2 presents briefly the study methodology. Section 3 reviews one-step denoising techniques by discrete wavelet transform. Section 4 devotes to issues related to the wavelet packet based iterative denoising. Section 5 surveys two wavelet-based signal processing and pattern recognition tools: XWT and spectral powers. Section 6 explains the general features of the periling tower and the corresponding ambient vibration tests. Section 7 presents a numerical benchmark problem to compare the performance of the one-step and iterative denoising methods. Section 8 presents the results of the signal enhancement and frequency detection of the recorded data from the ambient vibration test. The concluding remarks are presented in Section 8.

## 2. Proposed methodology

One-step wavelet-based denoising methods have been used widely for denoising data with different wavelet families, decomposition levels, and thresholding methods. Designing new wavelet families [39], new wavelet transforms, or thresholding [40-44] is still an open research area for system identifications. For high levels of noise, however, the one-step denoising methods may not be so effective, and so iterative filtering is suggested, e.g. [45]. In this study, there are high-level of noises mainly due to the rigidity of the structure, elevators, machinery operations, fans and considering wind for the ambient test. Hence, here, the iterative wavelet-based method would be used to reduce noise effects as much as possible. The iterative method would use the discrete wavelet packet method and the hard-thresholding approach. The main question is how to choose the threshold value which is proportional to the noise-variance. In general, the theoretical methods to estimate noise levels may lead to over- or under-estimated results. Hence, the empirical methods can be recommended [46,47].

Our experiments show that for wavelet-packet-based iterative denoising choosing of the proper proportional coefficient may not be feasible through empirical observations based on either SNR or peak SNR (PSNR) (which was proposed in [46] for the iterative method based on common discrete wavelet transform). Hence, a proper value may be estimated by the trial-and-error method.

By a benchmark problem, the robustness of the iterative method is studied. The problem is denoising a harmonic signal with high-level of noise with the wavelet-based one-step and the iterative schemes.

After iterative denoising and enhancements of initial data, the possible modal frequencies would be detected simultaneously by using complex CWT and corresponding power spectra in the wavelet spaces. The complex CWT reveals the frequency contents through time and variation pattern in time. For modal frequencies, such frequencies would continuously be excited during time. Also to capture more precisely



predefined threshold  $\varepsilon$ , detail coefficients smaller than this threshold are considered zero. The soft thresholding method can be used to prevent sudden jumps in the modified (thresholded) detail coefficients, which is defined as [26-28]:

$$\hat{d}(j, k) = \begin{cases} 0, & |d(j, k)| \leq \varepsilon, \\ \text{Sign}[d(j, k)][|d(j, k)| - \varepsilon], & |d(j, k)| > \varepsilon. \end{cases} \quad (1)$$

Other thresholding functions such as semi-soft and Garrote [29] can also be used to have a smooth transition in the threshold coefficients. The threshold value can be independent of the resolution level  $j$  or dependent on it. The independent level is known as global thresholding, where a predetermined threshold  $\varepsilon$  is used for all resolutions. But for the level-dependent case, for each resolution level, a different threshold is used, which is shown as  $\varepsilon_j$  for level  $j$  [28]. Several methods have been proposed to estimate the threshold value, such as: SURE, Universal and GCV (generalized cross-validation) [26-28]. Each of these approaches has its own concept to determine the threshold values, but all of them try to minimize the mean squared error,  $MSE(\varepsilon)$ . These three methods can be developed as global and level-dependent thresholds.

According to the number of denoising iterations on noisy data, two different approaches were developed: 1) one-step [24-29], and 2) iterative method, also known as layering method [30-36]. In the one-step method, noise is removed by one-step of thresholding (with a general or level-dependent threshold value), while in the iterative method, noise is removed iteratively and step by step, until satisfying a convergence criterion. In each iteration, the data is the noise obtained from the previous iteration [30-36].

Based on the concept of  $MSE$ , two criteria, the signal noise ratio (SNR) and the peak signal noise ratio (PSNR), have been used to determine the quality of various data enhancement methods (denoising). These two criteria can be defined as [27, 28]:

$$\begin{aligned} SNR &:= \frac{\text{Ave. signal power}}{\text{Ave. noise power}} = 10 \text{Log}_{10} \left[ \frac{\sigma^2(\hat{s})}{\sigma^2(s-\hat{s})} \right] = 10 \text{Log}_{10} \left[ \frac{\sigma^2(\hat{s})}{\sigma^2(\text{noise})} \right] \text{ (dB)}, \\ PSNR &= 10 \text{Log}_{10} \left[ \frac{\text{Max}(|\hat{s}_i|)^2}{\sigma^2(s-\hat{s})} \right] = 10 \text{Log}_{10} \left[ \frac{\text{Max}(|\hat{s}_i|)^2}{\sigma^2(\text{noise})} \right] \text{ (dB)}, \end{aligned} \quad (2)$$

where  $\hat{s}$  and  $s$  denote denoised and original (noisy) signals, respectively;  $\sigma^2(Z)$  is the variance of  $Z$ ;  $\hat{s}_i$  is the  $i$ th element of  $\hat{s}$ ; and  $\sigma^2(s - \hat{s})$  measures the variance of the noise:  $s - \hat{s}$ . Function  $R = \sigma^2(s - \hat{s})$  denotes the risk-function, which is equivalent to  $MSE$  [28]. The unit of measurement for both SNR and PSNR is dB (decibel). The parameter SNR measures the ratio of average power of a signal to average power of power. Also, PSNR measures the ratio between the maximum possible value of power of a signal and the power of noise. Hence, the larger values of the SNR and PSNR indicate the better performance of the denoising (or compression) methods, because these two parameters have inverse relationships with the noise variance ( $\sigma^2(s - \hat{s})$ ). For practical applications, values larger than 30 dB are recommended for PSNR.

#### 4. Iterative denoising based on wavelet packet transform

Despite the widespread use of one-step denoising methods for signal processing problems, this method may not lead to suitable results for highly noisy data. Iteration-based denoising methods have been developed to improve the results of one-step methods [30-36]. An iterative denoising approach is followed in this section to improve data with a high level of noise. For a noisy signal  $\mathbf{Z} = \{z[1], \dots, z[N]\}$ , assuming the signal  $\mathbf{Z}$  as noise is the first step of the iterative denoising algorithm. Then, coherence and significant features across the noise can be obtained.

Noise detection is performed by the decomposition of  $\mathbf{Z}$  by MRA (here by the wavelet packet transform), and then at the last level of resolution (with the coarsest resolution level  $j = J_{min}$  or  $J_{min} = 4$  in Fig. 1), those detail coefficients that are larger than a specified threshold (which represent important phenomena) are identified. Using the statistical approach, the distribution of detail coefficients  $d(J_{min}, k)$  is measured (at coarsest scale  $J_{min}$ ) and is shown by the variance of the detail coefficients, i.e.:  $(\sigma_n^{J_{min}})^2$ . Then, detail coefficients larger than  $C \times \sigma_n^{J_{min}}$  are assumed to belong to a considerable physical phenomenon, for  $C \geq 1$ . The selected detail coefficients with the (unchanged) scale coefficients at the coarsest resolution level  $J_{min}$  are reconstructed as the first estimate of the denoised signal, and the remaining of the detail coefficients along with zero scale coefficients are reconstructed and named as updated noise data. The denoised data at the end of each iteration is added to the denoised data obtained in the previous iteration. The above procedure is repeated for the new updated noise data in the next iteration. In fact, significant information is frequently removed from the initial data containing high-level of noise. In this regard, this approach is also known as the peeling method.

#### 5. Information detection of the enhanced data by continuous wavelet transform

In the previous section, the signal enhancement method was described based on the discrete wavelet packet transform. In this section, after improving the signal, the time-frequency information of the data can be studied and detected by using the CWTs, where for data  $f(t)$  and wavelet  $\psi(t)$ , CWT can be defined as:  $W_{\psi}f(a, b) = \frac{1}{\sqrt{|a|}} \int_{-\infty}^{+\infty} f(t) \psi^* \left( \frac{t-b}{a} \right) dt$ , where:  $a$  and  $b$  denote the scale and location parameters, respectively; and the symbol “\*” shows the imaginary conjugate of a function. This means by the continuous wavelet transform, a signal is watched locally with a moving window of different width (by moving  $\psi(t/a)$ ) Hence, localized information in time-frequency can be detected. In this work, the complex Merlot wavelet is used to detect instantaneous frequencies, defined as:

$$\psi(t) = \frac{1}{\sqrt{\pi \times v_b}} (e^{2\pi i v_c t} - e^{-v_b(\pi v_c)^2}) e^{-t^2/v_b} \quad (3)$$

where  $v_b$  denotes the bandwidth frequency and  $v_c$  is the central frequency. It is assumed that:  $v_b = 2$  and  $v_c = 1.10$ . Hence, the condition of complexity of the Merlot wavelet, that is  $\sqrt{v_b} v_c \geq \sqrt{2}$  would be satisfied. XWT and related spectral power are two powerful signal processing tools developed based on CWTs. At first, the concept of spectral power of wavelet transform is presented. This concept helps identify energy concentration in the frequency (or scale) domain. Spectral power is defined as follows:

$$P_W(a) = \frac{1}{L} \int_{t_0}^{t_0+L} |W_\psi f(a, b)|^2 db \quad (4)$$

where  $b$  represents the location of the scaled wavelets  $\psi(t/a)$ ;  $L$  denotes the duration of data.

### 5.1 XWTs and corresponding spectral powers

Two analyses that can be performed based on the coefficients of CWTs are: 1) XWTs and 2) Spectral power of XWTs. Regarding XWTs, in practical calculations, it is often effective to detect possible links between two signals. Based on the concept of XWT (denoted by  $XW_\psi$ ) energy coherence can be evaluated. For signals  $f(t)$  and  $g(t)$ ,  $XW_\psi(f, g)$  can be defined as [24]:

$$XW_\psi(f, g) = W_\psi f(a, b) \times W_\psi g(a, b)^* \quad (5)$$

In the above relation, the symbol “\*” represents the imaginary conjugate of a function. XWT identifies regions where two data have power (energy) coherence in frequency-time space. Due to the random nature of noise, it is expected that two recorded data, at different times and resolutions, have unrelated noise energies. Regarding the spectral power of XWTs, in identifying the energy coherence between two data in the frequency domain, the power of XWTs can be useful; the XWT power is defined as:

$$P_{XW}(a) = \frac{1}{L} \int_{t_0}^{t_0+L} |XW_\psi(f, g)| db \quad (6)$$

Identifying physical (real) phenomena in data is possible by simultaneously studying two powerful signal processing tools, that is XWTs and corresponding spectral powers. It can simultaneously show the continuous distribution/pattern of energies in the time-frequency representation by XWT energy and also the concentration of energies in the frequency domain by the corresponding spectral power.

## 6. Ambient vibration test on the Ammonium Nitrate prilling tower

The petrochemical complex, constructed in 1959, is placed 45 kilometers north of the city of Shiraz, Iran, near the Korr River. Geological studies have shown that the seismic activity in this zone is high, nevertheless, the risks resulting from geotechnical instability, including faulting, liquefaction, subsidence, landslide and falling rock, are low [48].

The Ammonium Nitrate Prilling Tower is made of a concrete structure and categorized as non-building industrial structures. Four steel shimmies with the height of 25m, diameter of 1.9m and thickness of 0.5cm are attached to the tower between the heights of 55.7m and 80.7m. Schematic illustration of the tower and the corresponding cross-section are presented in Fig. 2 [48].

Adjacent to the tower, the elevator's structure with rectangular section is located and locally attached to the tower at heights of 47.7, 50.6 and 55.7m. The foundation is constructed of reinforced concrete and contains a circular pile foundation with the thickness of 1.5m and 78 piles with the diameter of 60cm under the tower, and a rectangular pile foundation with the thickness 80cm and 27 piles of 60cm diameter under the elevator [48].

A typical accelerometer used for recording accelerations deduced by ambient vibrations is illustrated in Fig. 2(b). This device is a "Force Balance" type accelerometer, which has: (1) 100Hz bandwidth, (2) Variable and adjustable measurement range of +0.25 g to +4g, (3) Adjustable sensor sensitivity from +5V/g to +80V/g, and (4) Sensor dynamic range of 140dB.

Due to deterioration from its original condition and increasing vibrational response (mainly due to stiffness reduction), which leads to automatic equipment shutdown, the owners motivated for rehabilitation studies. The ambient vibration test is performed by the wind load. Spatial locations of sensors along the tower and recording directions "1" and "2" are illustrated in Fig. 2(d). Acceleration recorders on the tower are denoted by  $P_i$  where  $i \in \{1, \dots, 7\}$ , and the recorder  $R$  is the reference one. Recording directions for the recorded data at the main tower are denoted by  $k$  as  $P_{ik}$  for  $k \in \{1, 2\}$ . Data are recorded by the sampling step  $\Delta t = 1/100$  Sec [48].

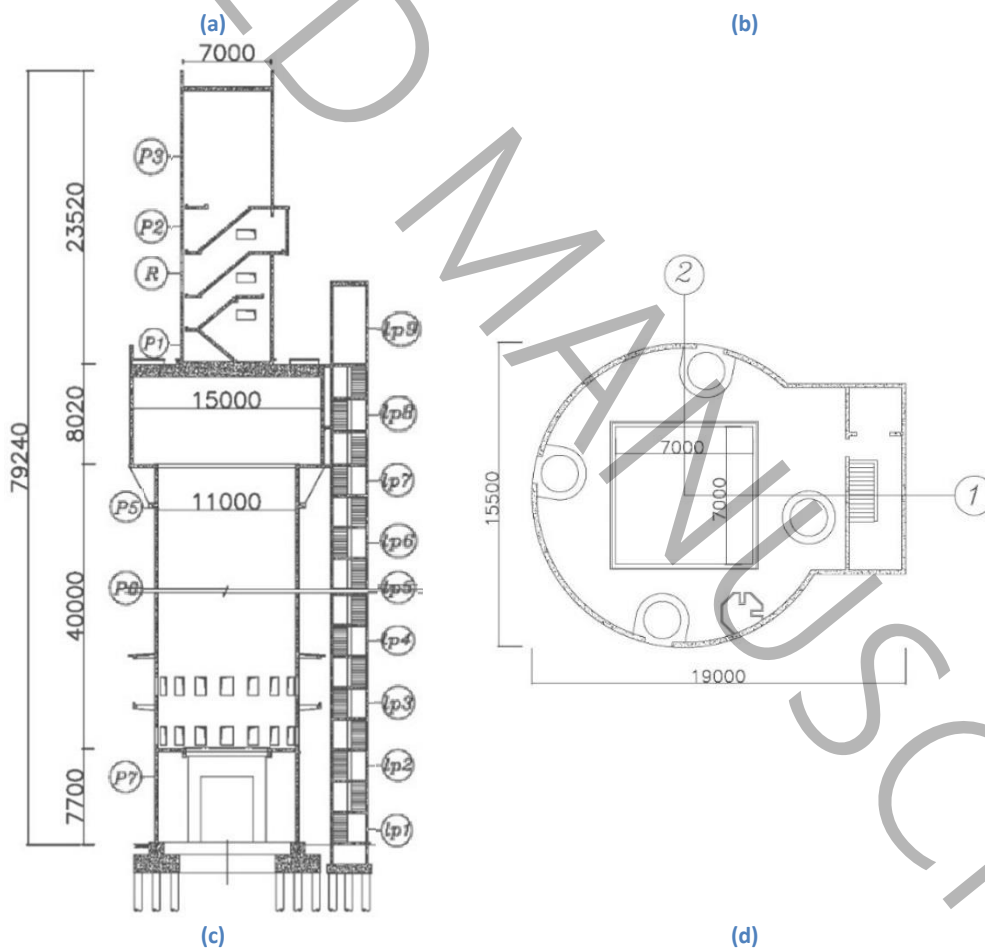


Fig. 2: Ammonium Nitrate periling tower, Shiraz, Iran; (a) Ammonium Nitrate periling tower, (b) A sensor on tower, (c) Locations of data recorders, (d) Recording directions "1" and "2" [48].

## 7. benchmark problems

In this section, the performance of the iterative denoising approach will be studied by two benchmark problems: one with one harmonic component and one with non-stationary chirp signal including three frequencies polluted with considerable noise levels.

**Benchmark 1:** Let us consider a harmonic function  $y_0(t) = \sin(6t)$  for  $0 \leq t \leq 2\pi$ , with the angular frequency  $\omega_0 = 6 \text{ rad/s}$ , or with the period  $T_0 = 2\pi/\omega_0 = 1.047$  second. A function with real random values belonging to  $[-5,5]$  (and with the uniform distribution) denoted by  $y_{noise}(t)$  is added to  $y_0(t)$ . The resulting function with the considerable noise is presented here by:  $y_1(t) = y_0(t) + y_{noise}(t)$ . These functions are illustrated in Fig. 3. The function  $y_1(t)$  is sampled with the time step  $dt = 0.005$ . The aim is denoising of the sampled  $y_1(t)$  by the common wavelet-based methods and the iterative scheme (based on the discrete wavelet transformation) and compare their performance with each other.

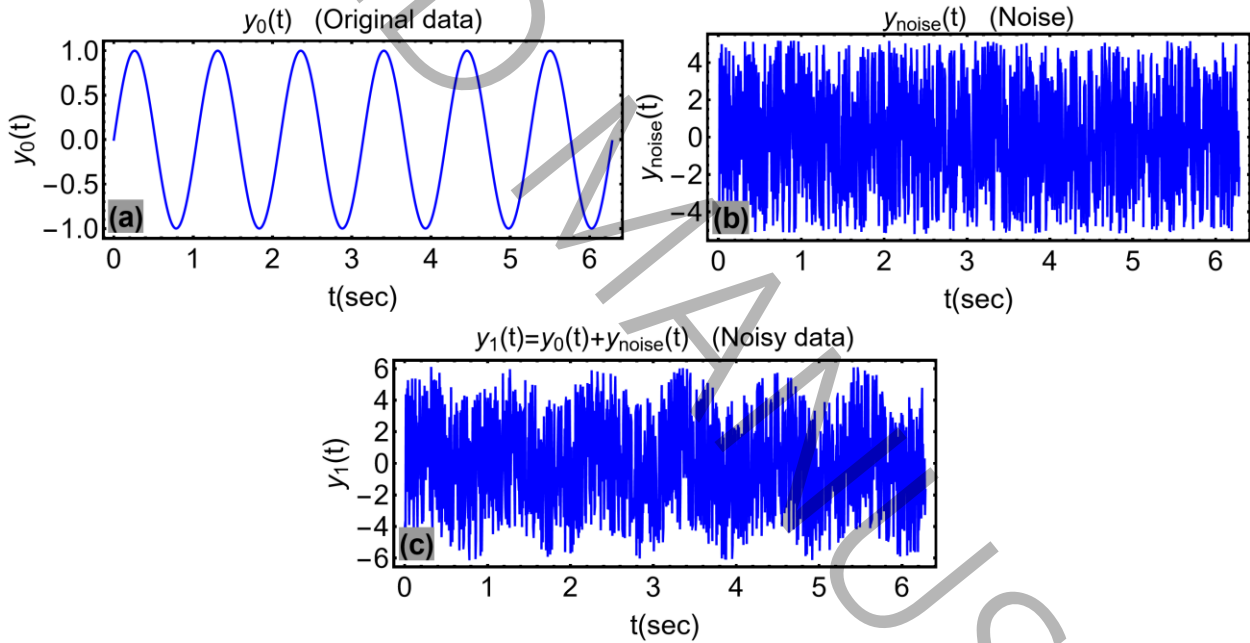


Fig. 3: The noisy data  $y_1(t)$  generated with the superposition of the harmonic data  $y_0(t)$  and the noisy data  $y_{noise}(t)$ ; (a) Original harmonic signal  $y_0(t)$ , (b) Random noise  $y_{noise}(t)$  with uniform distribution, (c) Noisy data  $y_1(t)$ .

The sampled noisy data is denoised with the common one-step discrete wavelet-based denoising method, with “Symlet-12” wavelet family, 10 decomposition levels and with three different thresholds obtained with three famous approaches, that is: the “SURE”, “Universal” and “Visu Shrink” approaches. The one-step denoised results are presented in Fig. 4. The results confirm that the one-step wavelet-based denoising leads to over- or under-smoothed results. The values of the SNR and PSNR are presented in Table 1. This table confirms that one or both values of SNR and PSNR are negative for the “Universal” and the

“VisuShrink” thresholds, which confirms these thresholds are improper. It is interesting that for the “SURE” threshold, despite the SNR and PSNR values are positive and large enough, however, the denoised result,  $\hat{y}(t)$  is incorrect (as it should approximate  $y_0(t)$ ). This confirms that controlling only the values of the SNR and the PSNR could not be enough.

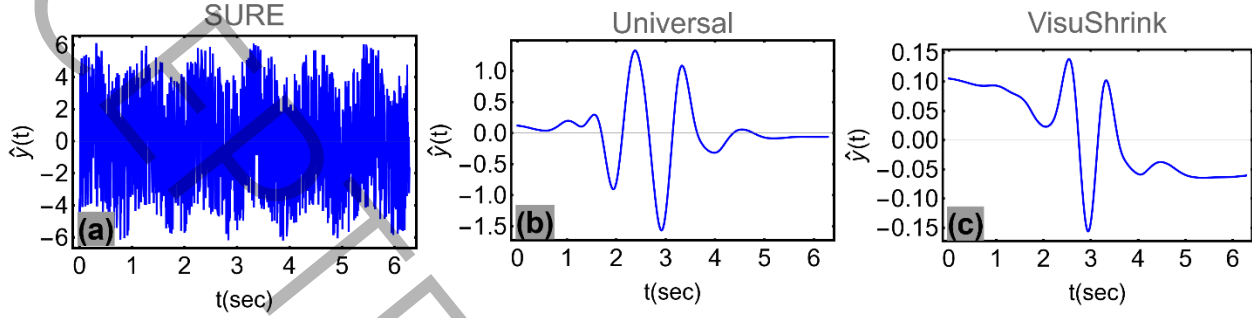


Fig. 4: The denoised results with the one-step wavelet-based method with three different threshold values; (a) Denoising with the SURE threshold, (b) Denoising with the Universal threshold, (c) Denoising with the VisuShrink threshold.

Table 1: Denoising of the signal  $y_1$  with different one-step wavelet-based denoising methods; where  $N_d = 10$

Method	$y_1$	
	SNR(dB)	PSNR(dB)
VisuShrink	-32.05799	-25.5346
SURE	30.9656	37.11068
Universal	15.3792	-5.3993

For the iterative method, it is assumed that: 1) Using of the “Symlet[12]” wavelet family, 2) Number of decomposition levels is 12, 3) Number of iterations is four, 4) the threshold value for each iteration is  $\epsilon = 2.5\sigma$ , where  $\sigma$  denotes the variance (since noise level is high, a large value for  $\epsilon$  is chosen). For each iteration, the captured data (denoted by “Signal[i]”) and remaining noise (denoted by “Noise”) are presented in Fig. 5.

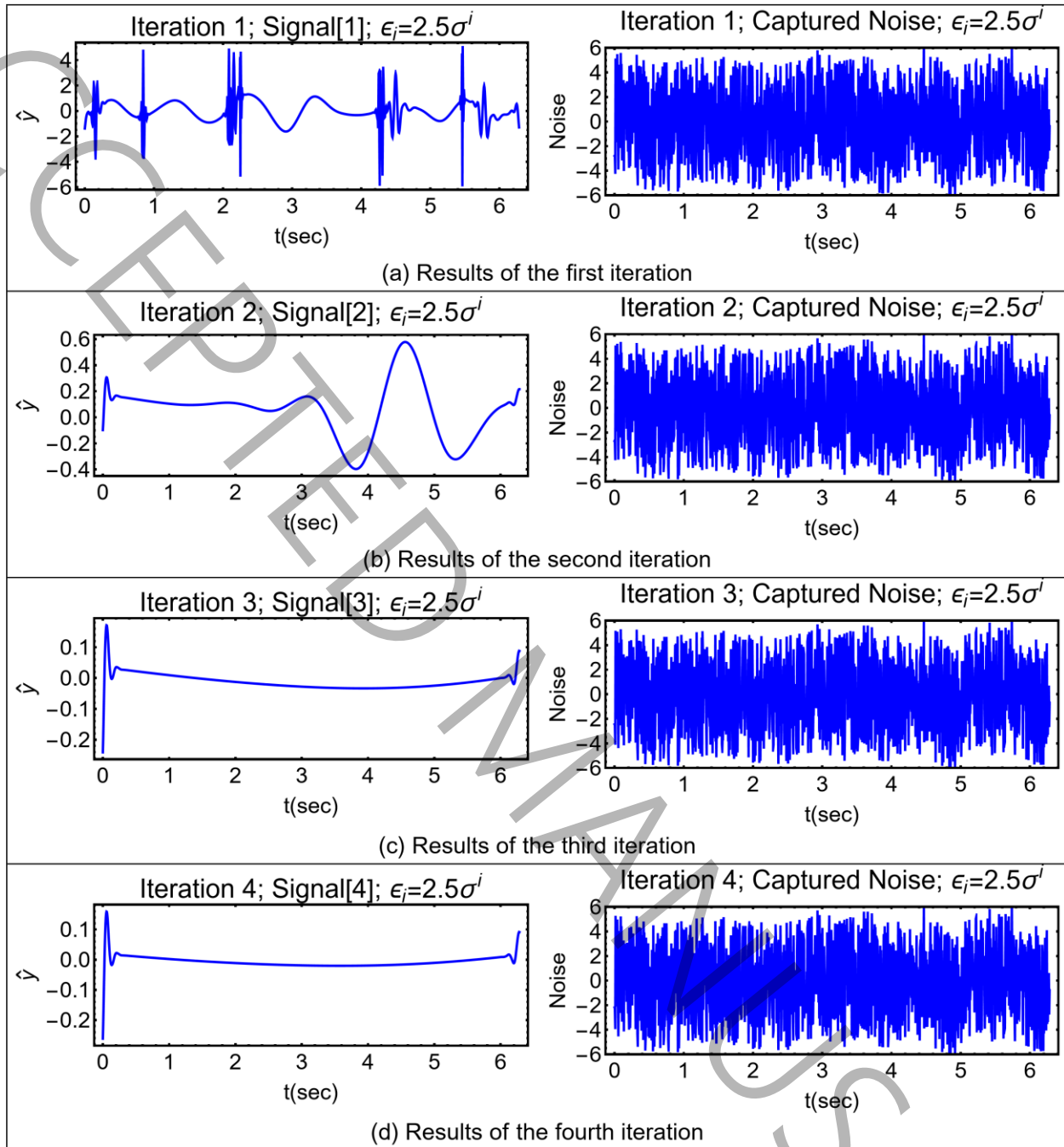


Fig. 5: Captured data and remaining noise at each iteration step. Iteration numbers are four.

By superposition of these four captured data (“Signal[1]” to “Signal[4]”), the final enhanced data can be evaluated. The difference between initial data ( $y_1(t)$ ) and the enhanced data is known as the final noise. The enhanced data and the final noise are presented in Fig. 6. After enhancement, the total pattern of  $y_0(t)$  can be estimated while it includes localized noises.

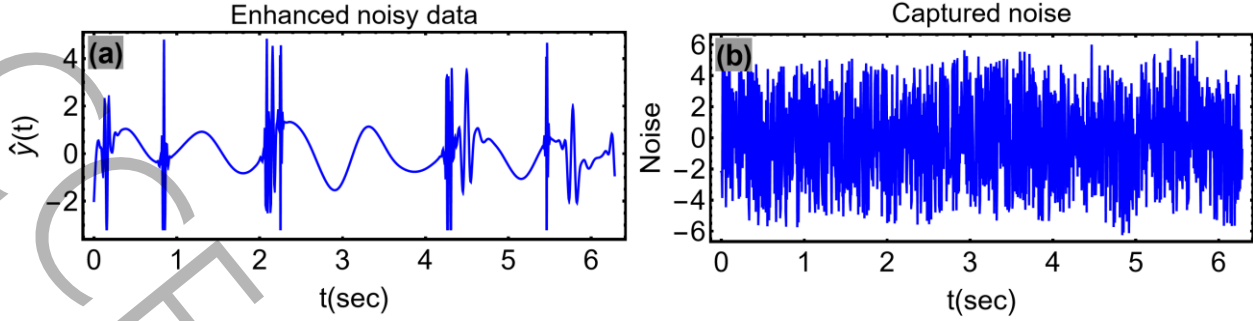


Fig. 6: The final results after four iterations with  $\epsilon_i = 2.5\sigma_i$ ; (a) The final enhanced data, (b) The remaining noise.

Using the continuous wavelet transform, denoted here by  $W_\psi$ , the values of  $|W_\psi|$  at different times and periods are presented for both the noisy data  $y_1(t)$  and the final enhanced data in Fig. 7. Where the wavelet family is the complex Morlet wavelet with parameters  $\nu_b = 2$  and  $\nu_c = 1.10$ . This figure confirms: 1) For the  $y_1(t)$  the frequency components cannot be detected, and nearly all frequency bands are polluted, 2) For the enhanced data, the frequency content is approximately around the period  $T \approx 1.06 \text{ sec.}$ : very close to the frequency content of  $y_0(t)$ . Also, the effects of considerable noise can nearly be removed from the noisy data  $y_1(t)$ .

This benchmark problem confirms the robustness of the iterative denoising approach for data with high-level of noise. Also, this approach can be used for data with localized high-level of noise.

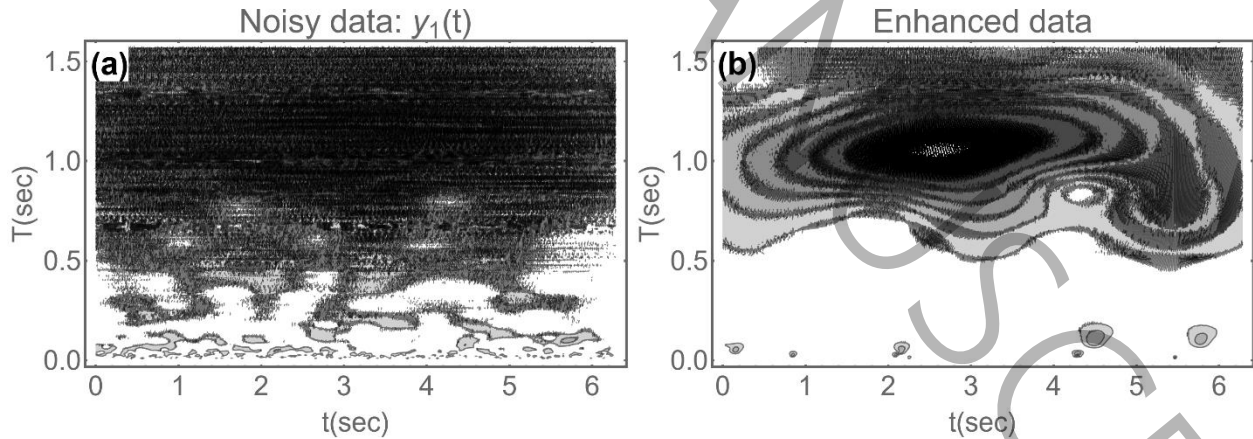
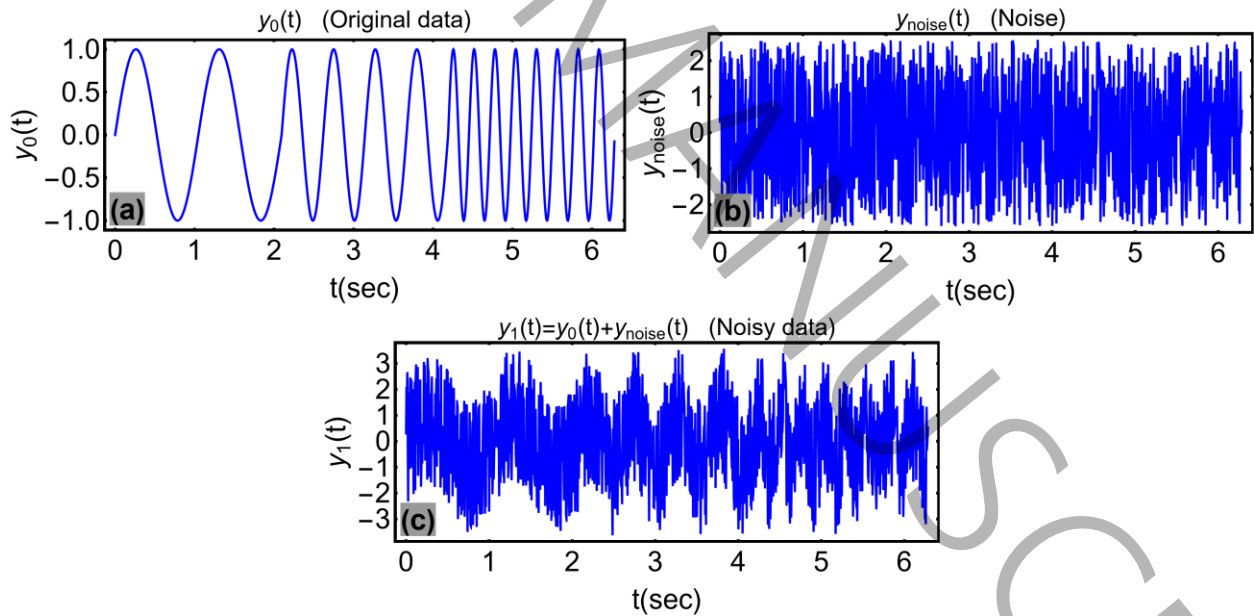


Fig. 7: The absolute values of CWTs,  $|W_\psi|$ , obtained by the complex Morlet wavelet, where “T” denotes the period; (a)  $|W_\psi|$  for the noisy data, (b)  $|W_\psi|$  for the enhance data.

**Benchmark 2:** Let us assume a chirp function, as:  $y_0(t) = \sin(6t)$  for  $0 \leq t \leq \frac{1}{3}2\pi$ ;  $y_0(t) = \sin(12t)$  for  $\frac{1}{3}2\pi \leq t \leq \frac{2}{3}2\pi$ ; and  $y_0(t) = \sin(24t)$  for  $\frac{2}{3}2\pi \leq t \leq 2\pi$ . A function with real random values belonging to  $[-2.5, 2.5]$  (and with the uniform distribution) denoted by  $y_{noise}(t)$  is added to  $y_0(t)$ . The periods of the signal are: For  $0 \leq t \leq \frac{1}{3}2\pi$ ,  $\omega_0 = 6 \text{ rad/s}$ , or  $T_0 = 2\pi/\omega_0 = 1.047$  second; For  $\frac{1}{3}2\pi \leq t \leq \frac{2}{3}2\pi$ ,  $\omega_0 = 12 \text{ rad/s}$ , or  $T_0 = 0.5235$  second; For  $\frac{2}{3}2\pi \leq t \leq 2\pi$ ,  $\omega_0 = 24 \text{ rad/s}$ , or  $T_0 = 0.2618$  second.

The polluted signal is denoted here by:  $y_1(t) = y_0(t) + y_{noise}(t)$ . These functions are illustrated in Fig. 8. The function  $y_1(t)$  is sampled with the time step  $dt = 0.005$ . The aim is to enhance the signal  $y_1(t)$  by the iterative scheme via the discrete wavelet transform. All assumptions for the wavelet transform are the same as Benchmark 1.

For  $i$  th iteration, the captured data (denoted by “Signal[ $i$ ]”) and remaining noise (denoted by “Noise”) are presented in Fig. 9 for four iterations with the threshold  $\epsilon_i = 2.5 \sigma_i$ .



**Fig. 8:** The noisy data  $y_1(t)$  generated with the superposition of the harmonic data  $y_0(t)$  and the noisy data  $y_{noise}(t)$ ; (a) Original chirp signal  $y_0(t)$  including three harmonics, (b) Random noise  $y_{noise}(t)$  with uniform distribution, (c) Noisy data  $y_1(t)$ .

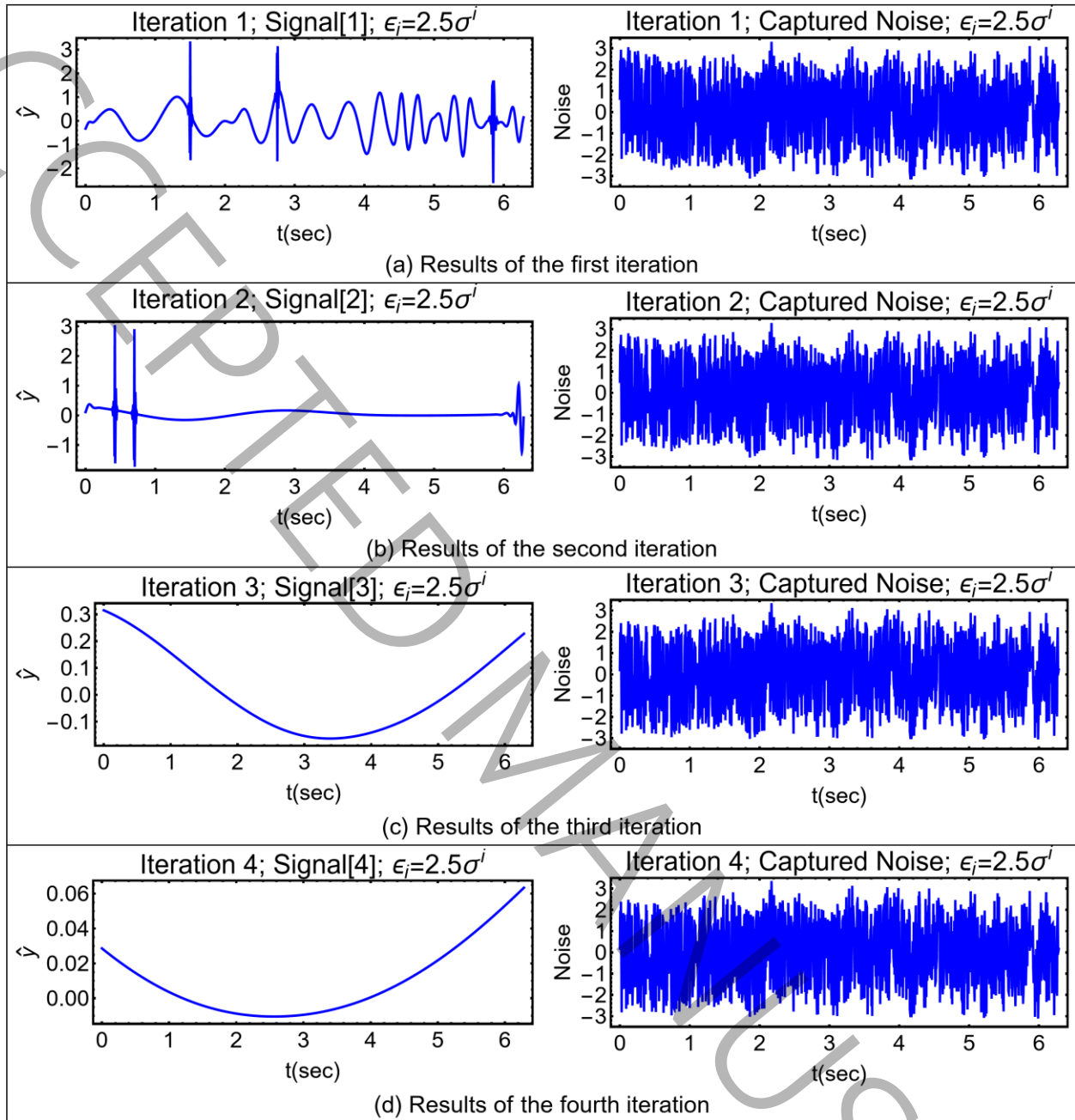


Fig. 9: Captured data and remaining noise at each iteration step. Iteration numbers are four.

By superposition of the four captured data (“Signal[1]” to “Signal[4]”), the final enhanced data can be calculated. The difference between initial data ( $y_1(t)$ ) and the enhanced data is known as the final noise. The enhanced data and the final noise are presented in Fig. 10. After enhancement, the total pattern of  $y_0(t)$  can be estimated while it includes localized noises.

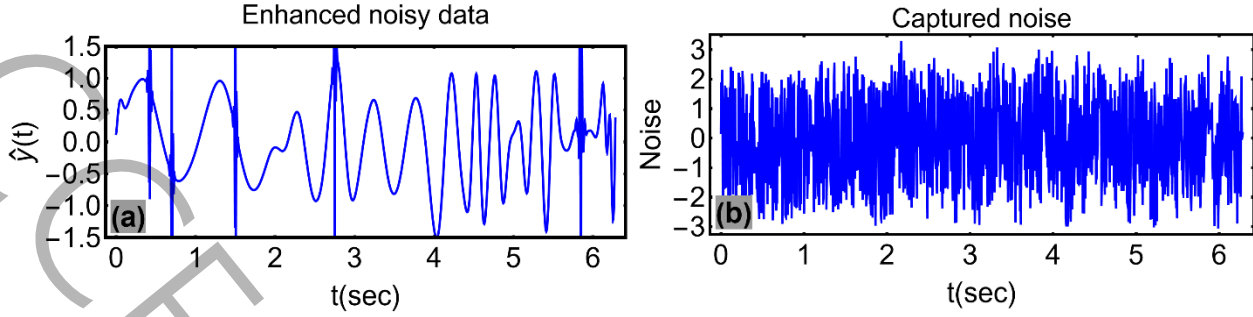


Fig. 10: The final results after four iterations with  $\epsilon_i = 2.5\sigma_i$ ; (a) The final enhanced data, (b) The remaining noise.

By the complex continuous wavelet transform (i.e.,  $W_\psi$ ), the values of  $|W_\psi|$  at different times and periods are presented for both the noisy data  $y_1(t)$  and the final enhanced data in Fig. 11. The complex Morlet wavelet is used for the transformation with parameters  $\nu_b = 2$  and  $\nu_c = 1.10$ . This figure confirms: 1) For the  $y_1(t)$  the frequency components cannot be detected, and nearly most frequency bands are polluted, 2) For the enhanced data, the periods  $T = 1.047$ ,  $T = 0.5235$ , and  $T = 0.2618$  are denoted by the blue dashed lines in Fig. 11(b) which are the period contents of the original data  $y_0(t)$ . It is obvious that the enhanced signal has effective concentrations around the periods  $T = \{1.047, 0.5235, 0.2618\}$ .

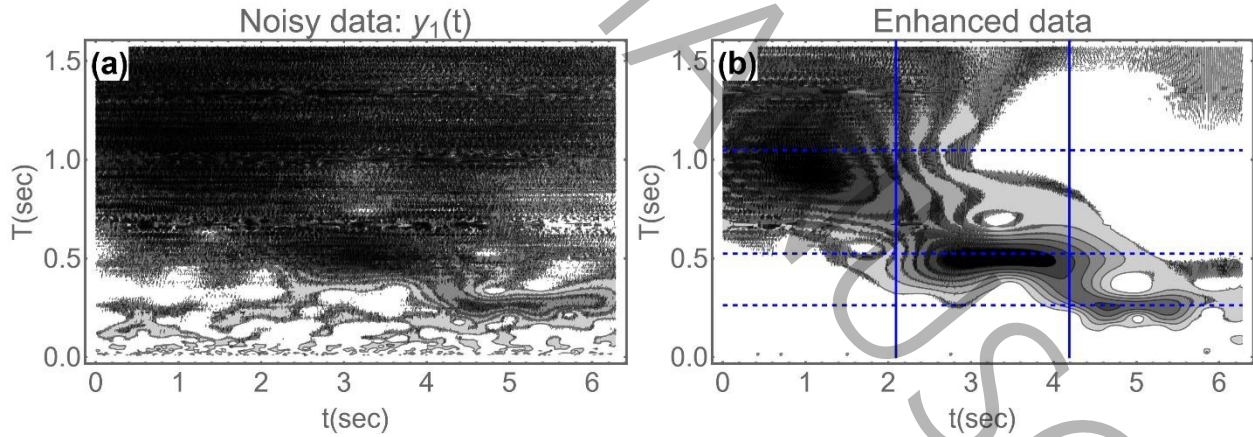


Fig. 11 The absolute values of CWTs,  $|W_\psi|$ , obtained by the complex Morlet wavelet, where “T” denotes the period; (a)  $|W_\psi|$  for the noisy data, (b)  $|W_\psi|$  for the enhance data; The horizontal dashed lines denote the periods 1.047, 0.5235, and 0.2618 seconds.

## 8. Results of estimated modal frequencies from the ambient vibration test

Different recorded data in the main tower, P21, P31, P51, P12 and P72, are presented in Fig. 12. Here, the sampling time step is  $\Delta t = 0.01$  and the data lengths are chosen to be  $L = 80$ .

Indeed, to distinguish two nearly located separate peaks of frequencies  $f_1, f_2$ , where  $f_2 > f_1$  it is necessary to use a data length  $L$ , or truncate the original signal by length  $L$ , as [49]:

$$L \geq \frac{2}{f_2 - f_1} \quad (7)$$

or:

$$\Delta f = f_2 - f_1 \geq \frac{2}{L} \quad (8)$$

Hence in our study, the peaks with difference  $\Delta f = \frac{2}{80} = 0.025$  (Hz) can be distinguished. Hence, the longer the length of data, the more accurate frequency detection.

At first, two common approaches are considered to detect modal frequencies: 1) Studying in the Fourier space, 2) Investigating by the one-step denoising in the wavelet space by the discrete wavelet transform.

Regarding the Fourier domain, the frequency content of the signals P21, P31 and P51 are studied by using the discrete Fourier transform, denoted here by  $\mathcal{F}(\cdot)$ . The energy densities in the frequency domain,  $|\mathcal{F}(y)|^2$  are presented in Fig. 13. It is obvious that due to the ambient vibration, operations of mechanical systems, elevators, fans and back-ground noise, there are several peaks. Also, due to the lack of information from time domain, it is impossible to select modal frequencies directly from the frequency peaks.

### 8-1: One-step denoising methods based on wavelet (packet) transform

Different steps of wavelet-based denoising by the one-step methods can be summarized as: 1) *Estimation* of noise level in a process; 2) *Modification* of detail coefficients  $\{d(j, k)\}$  where the modified set is denoted by  $\{\hat{d}(j, k)\}$ : where  $j$  and  $k$  denote resolution-level and position, respectively (with location  $k/2^j$ ); also  $j = \{J_{max} - 1, \dots, J_{min}\}$  where  $J_{max}$  and  $J_{min}$  represent the finest and the coarsest resolution-levels, respectively; 3) *Reconstruction* of the denoised signal by both  $\{\hat{d}(j, k)\}$  and the unchanged scale coefficients  $\{c(J_{min}, l)\}$  [50,51].

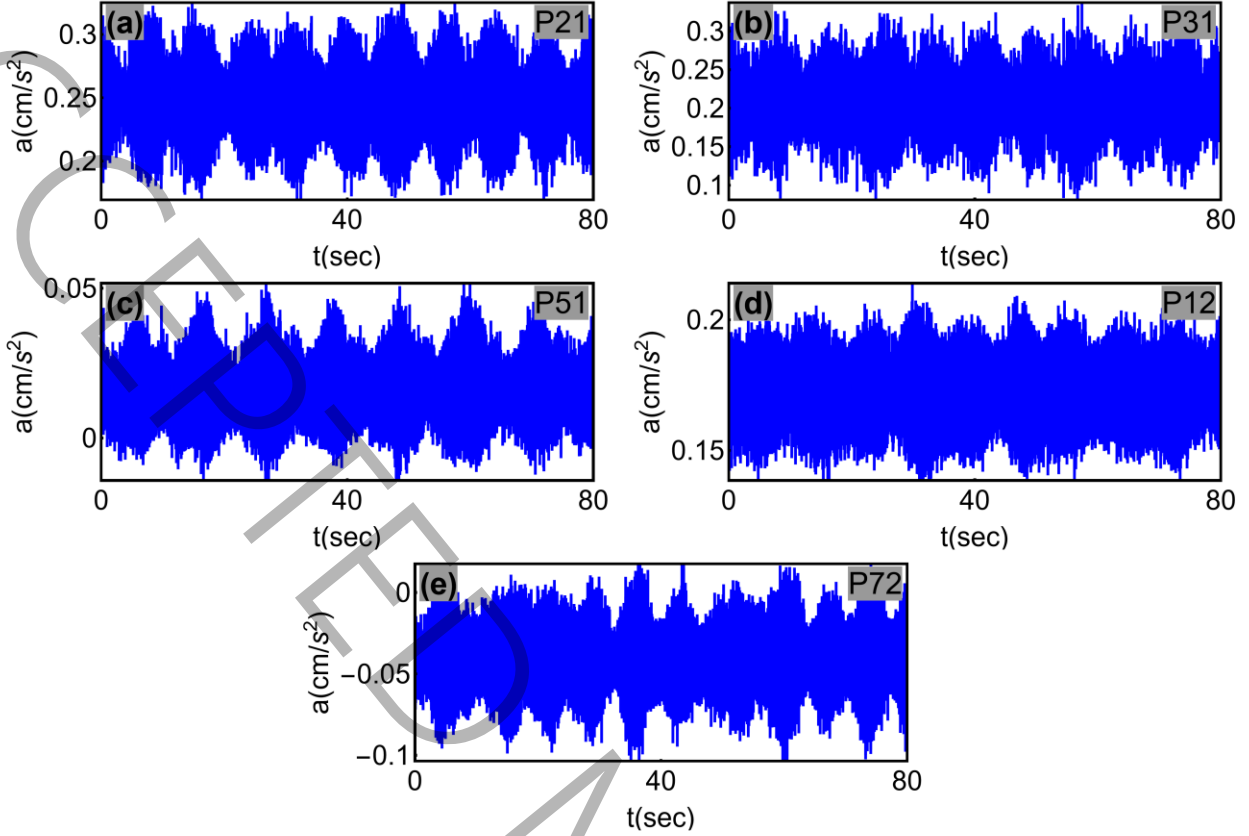


Fig. 12: Recorded signals at different stations. The horizontal and vertical axes denote time and acceleration, respectively; sampling time step is  $\Delta t = 0.01$ ; (a) Signal P21, (b) Signal P31, (c) Signal P51, (d) Signal P12, (e) Signal P72 [48].

The modifying stage can be performed by thresholding technique. For instance, for a pre-defined threshold “ $\epsilon$ ”, detail coefficients below this threshold are set to zero. This simple kill-or-keep method is known as the hard thresholding [50-52], with the definition:

$$s_{\epsilon}(w) = \begin{cases} 0, & |w| \leq \epsilon \\ w, & |w| > \epsilon \end{cases} \quad (9)$$

where  $s_{\epsilon}(\cdot)$  denotes the shrinkage function. To prevent sudden jump in modified (thresholded) detail coefficients, there is another simple and famous approach known as the soft thresholding method, defined as Eq. (1) [50-52].

The possible thresholding approaches are mentioned in Table 2. Regarding this table, the parameters can be defined as follows: The term “level” indicates a level-dependent thresholding. The Universal, SURE and GCV thresholding methods try to minimize the mean square error  $MSE(\epsilon) = \|\mathbf{f}_{\epsilon} - \mathbf{f}\|^2/N$ , where  $\mathbf{f}_{\epsilon}$  is a vector of thresholded data with the threshold value  $\epsilon$ ,  $\mathbf{f}$  is the unknown smooth (untouched or without noise) data, and  $N$  denotes the length of data. Since  $\mathbf{f}$  is unknown, it is necessary to estimate  $MSE$  [52].

In the Universal method (proposed by Donoho and Johnstone), the threshold gives a minimax solution of the ideal mean squared error in the asymptotic behavior of  $MSE$  (as  $N \rightarrow \infty$ ) [50-53]. For a signal of length  $N$ , for the Universal approach, the threshold is [29]:

$$\varepsilon \equiv \varepsilon_{\text{Universal}} = \hat{\sigma} \sqrt{2 \text{Log}(N)} \quad (10)$$

where  $\hat{\sigma}$  denotes the noise level or  $\hat{\sigma}^2$  is the noise variance for white Gaussian noise, which can be estimated as [29]:

$$\hat{\sigma} = \frac{\text{median}\{|d(J_{\max-1}, k)|: k = 1, 2, \dots, N/2\}}{0.6745} \quad (11)$$

where  $d(J_{\max-1}, k)$  denotes the detail coefficient at the first level of decomposition (or at the finest resolution  $1/2^{J_{\max-1}}$  with the location  $k/2^{J_{\max-1}}$ ). For large values of  $N$ , the Universal threshold can remove both the noise and the physical signal.

In the ‘‘SURE’’ method, the Stein’s unbiased risk estimator (SURE) is used for  $MSE$  estimations [50-52, 54].

For the case where the wavelet detail coefficients are sparse, Donoho and Johnstone show that a hybrid method which combines the Universal and the SURE thresholds is preferable than SURE. This hybrid threshold when used with the soft-thresholding method is known as the ‘‘SUREShrink’’ method. This threshold can be obtained as [55]:

$$\varepsilon \equiv \varepsilon_{\text{SUREShrink}} = \min\{\varepsilon_{\text{SURE}}, \hat{\sigma} \sqrt{2 \text{Log}(N)}\} \quad (12)$$

Asymptotically, the generalized cross validation (GCV) function is a vertical translation of the  $MSE$  function, while the GCV can be evaluated only based on input (noisy) data. Hence, the threshold value minimizing GCV also minimizes  $MSE$  [52].

The ‘‘VisuShrink’’ threshold is designed to remove Gaussian noise with high probability (which tends to result in overly smooth image appearance). For image processing, by specifying a smaller sigma than the true noise standard deviation  $\hat{\sigma}$ , a more visually agreeable result can be achieved [56].

Regarding the common wavelet-based approach, in the following, the one-step denoising by the discrete wavelet will be studied for data P12. The famous approaches are used to select proper thresholds, that is: the ‘‘SUREShrink’’, ‘‘SURE’’, and ‘‘Universal’’ methods, see Table 2 for definitions. Using the Symlet[12] orthogonal wavelet with 13 decomposition levels, the denoised results are presented in Fig. 14. Also, the

values of SNRs and PSNRs of denoised data are presented in Table 3. The results confirm that: 1) The denoised data are over- or under-smoothed, 2) The negative values for either SNR or PSNR confirm improper denoising results.

In the following more advanced wavelet transform will be used, that is the wavelet packet transform to have considerable flexibility in studying locally in time-frequency spaces. For the P12 signal, the one-step denoised results by the wavelet-packet transform are presented in Fig. 15. The considered wavelet is *Symlet*[12] and  $N_d = 13$  (number of decomposition levels). The performance of different one-step denoising methods for P12 and P51 signals measured by SNR and PSNR criteria is also presented in Table 4. Both Fig. 15 and Table 4 show that among the denoising methods, the GCV denoising method leads to the best results. However, for all denoising methods the PSNRs are considerably less than 30 dB which confirms the insufficient performance of the one-step denoising method using different thresholding approaches.

**Table 2: Different denoising approaches with corresponding thresholding method and estimating noise level**

Denoising method	Thresholding approach	Estimating method of the noise level
GCV	soft	GCV
GCVLevel	soft	GCV-Level
SURE	hard	SURE
SURELevel	hard	SURE-Level
SUREShrink	soft	SURE
Universal	hard	Universal
UniversalLevel	hard	Universal-Level
VisuShrink	soft	Universal
VisuShrinkLevel	soft	Universal-Level

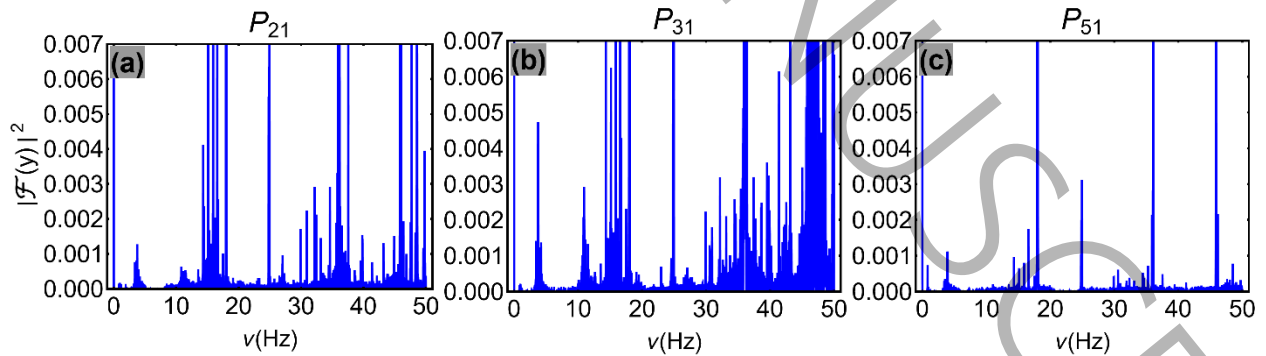


**Fig. 13: The energy density  $|\mathcal{F}(y)|^2$  in the frequency domain for different recorded data, where  $\mathcal{F}(y)$  denotes the Fourier transform of  $y(t)$ ; (a)  $|\mathcal{F}(y)|^2$  of signal P21, (b)  $|\mathcal{F}(y)|^2$  of signal P31, (c)  $|\mathcal{F}(y)|^2$  of signal P51.**

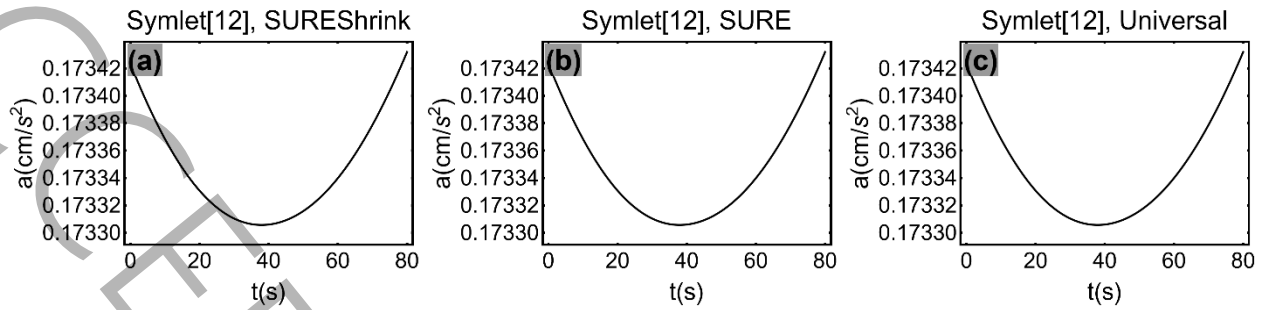


Fig. 14: The denoised P12 signal by the one-step wavelet based denoising using the thresholds obtained by the “SUREShrink”, “SURE” and “Universal” approaches, the Symlet-12 wavelet and  $N_d = 13$ ; (a) Over smoothed by “SUREShrink” threshold, (b) Over smoothed by “SURE” threshold, (c) Over smoothed by “Shrink” threshold.

Table 3: Denoising of the P12 signal with different one-step wavelet-based denoising methods; where  $N_d = 13$ .

Method	P12	
	SNR (dB)	PSNR (dB)
<i>SUREShrink</i>	-51.2786	22.2520
<i>SURE</i>	-51.2786	22.2521
<i>Universal</i>	-51.2787	22.2521

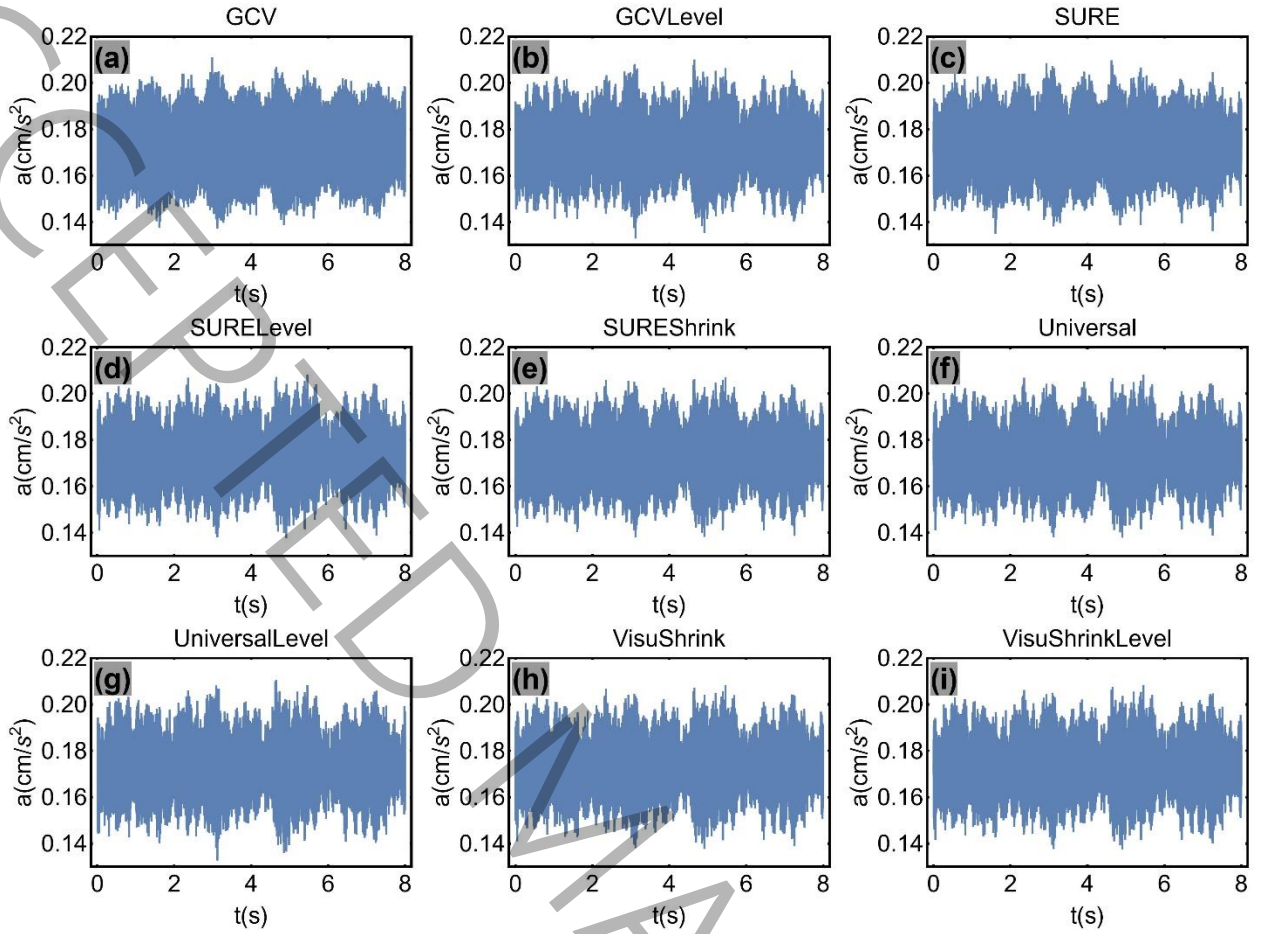


Fig. 15: Denoising of the P12 signal with different one-step wavelet-packet-based denoising methods; where  $N_d = 13$ .

## 8-2 Results for the Iterative denoising method based on wavelet packet transform

In this part, the results of signal enhancement with iterative denoising methods are presented. The largest possible value of  $C_n^j$  is obtained by a trial-and-error approach. The proper value of  $C_n^j$  is estimated as:  $C_n^j = 1$ . For signals P12 and P51, after 13 decomposition levels and 2 iterations, the values of the SNR and PSNR (which shows the effectiveness of the data enhancement method) are presented in Table 5. The *Symlet* wavelet of order 12 is assumed. Note that at the end of the iteration, the corresponding enhanced results and the initial noisy data are used in the calculation of the SNR and PSNR parameters.

Table 4: Effects of denoising with different thresholding by the one-step DWPT method with the *Symlet*[12] and  $N_d = 13$ .

Method	P12		P51	
	SNR (dB)	PSNR (dB)	SNR (dB)	PSNR (dB)
<i>GCV</i>	42.693504	18.560875	30.779994	16.993771
<i>GCVLevel</i>	32.025807	7.2176840	27.396521	13.593568
<i>SURE</i>	33.036281	8.6313331	25.231523	11.313871
<i>SURELevel</i>	30.054381	5.1049236	23.358374	9.4540047
<i>SUREShrink</i>	31.176870	6.3329708	24.243898	10.315175
<i>Universal</i>	30.3283032	5.4488797	25.048999	11.119087
<i>UniversalLevel</i>	30.6195054	5.6516937	24.081426	10.025114
<i>VisuShrink</i>	30.0684292	5.1165927	23.967897	10.051441
<i>VisuShrinkLevel</i>	30.2468347	5.2791582	23.683542	9.7212105

For the P12 signal, after each iteration, both noise and the captured (denoised) data (denoted as “Signal[i]”) are presented in Fig. 16. Number of iterations is two, and it is assumed:  $C_n^j = 1$  and  $N_d = 13$ . The last row presents the denoised (enhanced) signal after two iterations, obtained as:  $\sum_{i=1}^2 \text{Signal}[i]$ , see Fig. 16. Estimated noise is obtained from the difference of the initial signal P12 and the final enhanced data, as:  $\text{Noise} = P12 - \sum_{i=1}^2 \text{Signal}[i]$ . In each iteration, information with coherent structures is selected as denoised signal and the remaining data is used as noise and is used for the next iteration. In summary, due to the high-level of noise in the data, the noise cannot be removed completely. Indeed, it is removed as much as possible, by decomposing the signals into coherent (denoised signal) and incoherent (noise) structures by a method that is simultaneously localized both in time and frequency domains. The enhancement effect is investigated for P12 data.

The final energy density of noise (the final noise in Fig. 16, the last row) is presented on Fig. 17 in time-frequency representation by using the continuous wavelet transform to identify localized random-wise information in the noise. Fig. 17(a) represents a 3D plot of the information  $(t, T, |W_\psi|^2)$ , and Fig. 17(b) represents the corresponding contour plot, where  $t$  and  $T$  denote time and period, respectively; and  $|W_\psi|^2$  is energy density. All calculations are performed with the complex Morlet wavelet with parameters  $v_b = 2$  and  $v_c = 1.10$ . The energy range is  $0.02 \text{Max}[|W_\psi|^2] \leq |W_\psi|^2 \leq \text{Max}[|W_\psi|^2]$  in Fig. 18.

According to Fig. 18, for short periods, i.e.  $T < 0.5$ , stochastic like localized information exists and for periods in the range  $0.9 < T < 1.4$ , several significant phenomena occur locally, which may be caused by the operations of mechanical systems, elevators, and fans in the tower. This stochastic or local like information is not important in this study, since only excited modal frequencies are important with continuous presence through time. So far, several powerful signal processing tools have been used to enhance or clean the signal. After enhancing the data, in the next step, it is tried to integrate possible physical

features to extract more reliable information. The main idea is to use cross-wavelet analysis to find repeating physical patterns in different data.

**Table 5: Iterative denoising of data P12 and P51 with parameters:  $C_n^j = 1$  and  $N_d = 13$ .**

Iteration	P12		p51	
	SNR (dB)	PSNR (dB)	SNR (dB)	PSNR (dB)
1	28.820625	15.012432	36.564065	12.582310
2	39.730155	25.878075	45.793346	21.754959

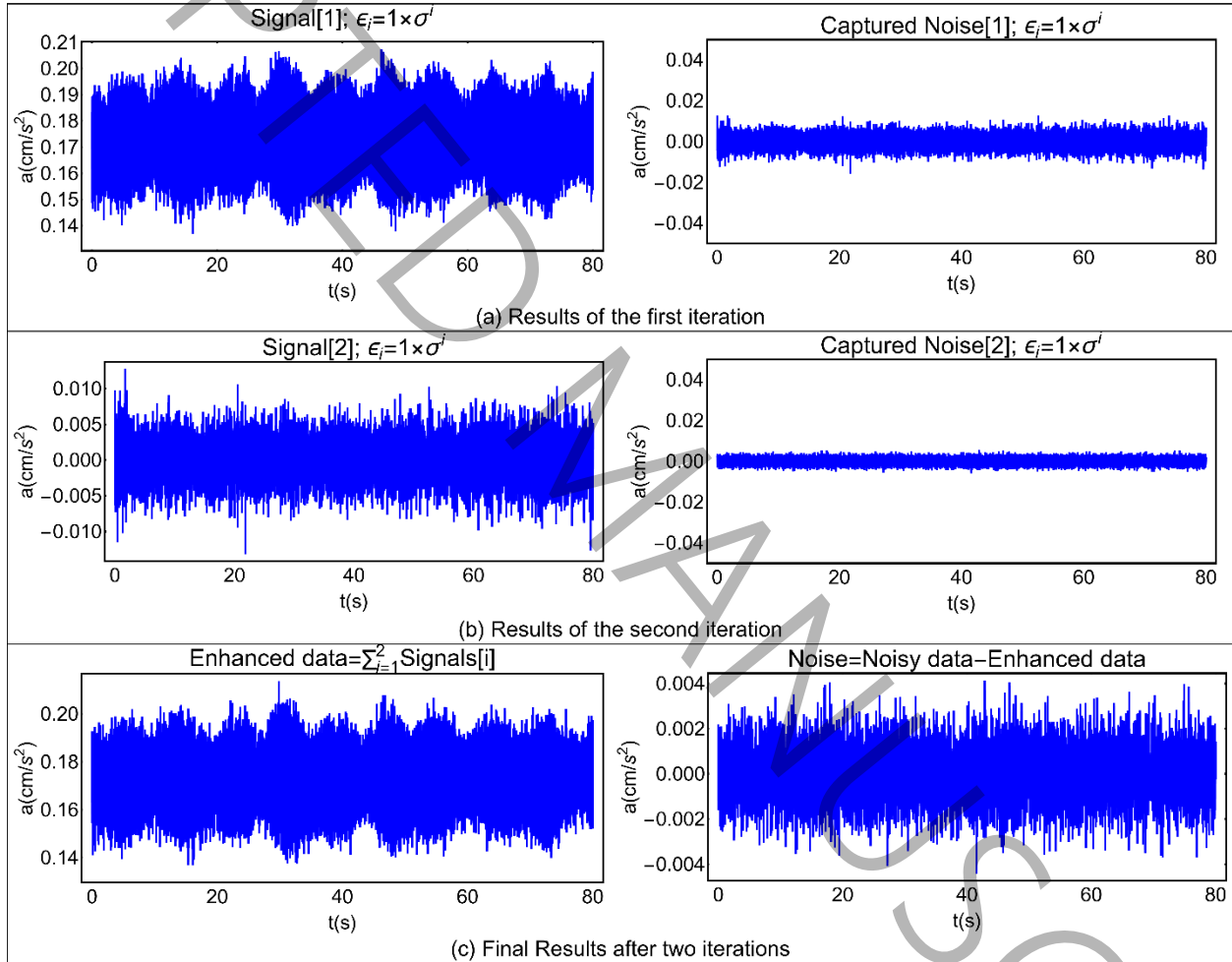


**Fig. 16: Iterative denoising of the signal P12 with two iterations; both denoised signal and estimated noise are provided at each iteration (the first row). The last row contains final denoised signal and estimated noise; evaluations are obtained with: *Symlet*[12],  $C_n^j = 1$  and  $N_d = 13$ .**

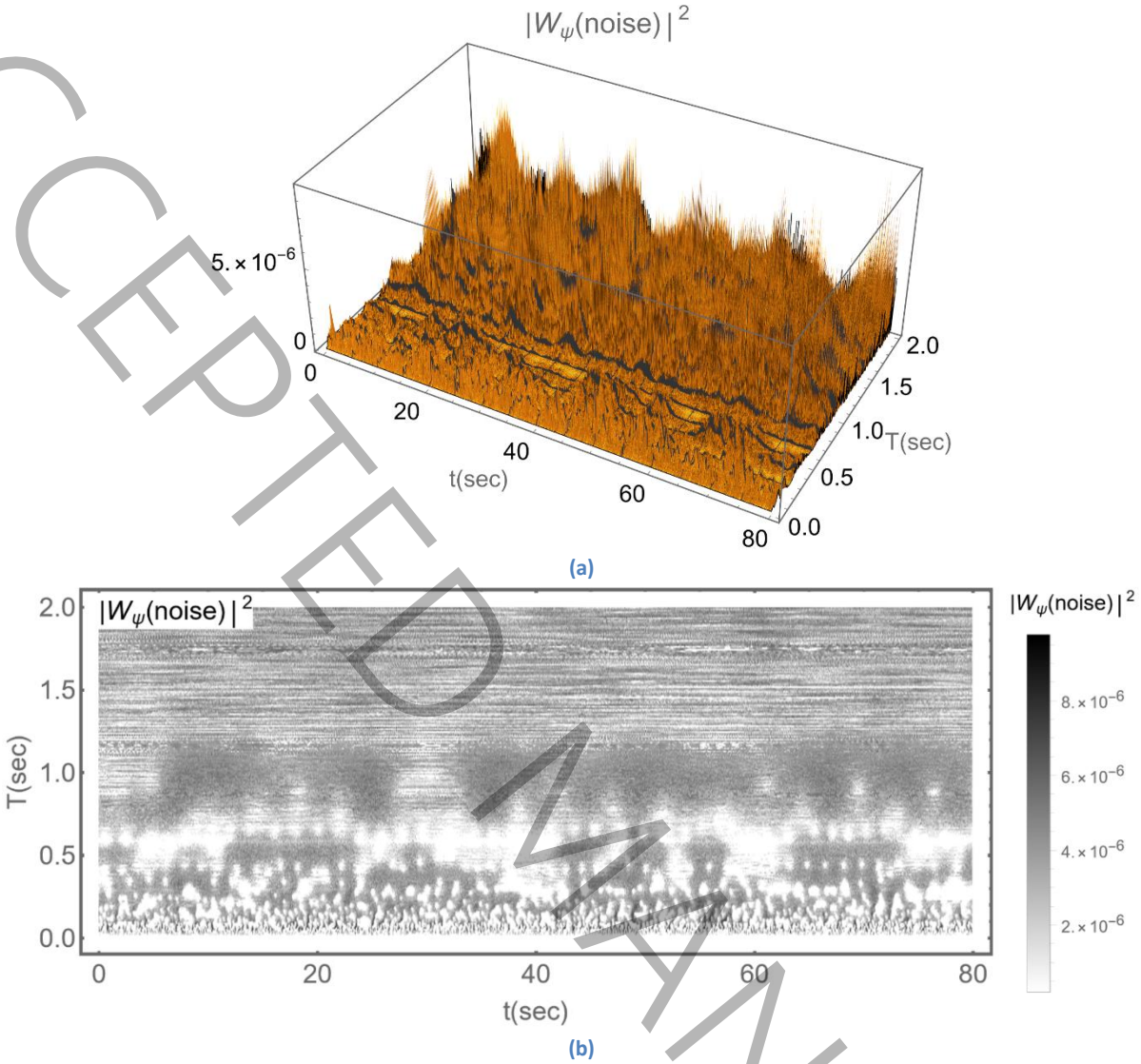


Fig. 17: Density of energy for the remaining noise after 13 iterations of the peeling algorithm for data P12 where  $C_n^j = 1$  and  $N_d = 13$ . (a) 3D representation of the noise energy density; (b) Corresponding contour-plot. Parameters “ $t$ ” and “ $T$ ” denote the time and period, respectively.

### 8-3 Cross-wavelet analysis for frequency detection

Here, by using cross wavelet analysis and corresponding power spectrum, physical responses are detected. Cross-wavelet transform can be used to identify common frequencies between two data with significant power. This feature of cross-wavelet analysis is used to study each pair of enhanced signals {P21, P31}, {P21, P51}, {P12, P72}, and {P21, P12}. Here, P21 is chosen as the reference record. These signals are denoised with the wavelet-packet based iterative scheme with *Symlet*[12],  $N_d = 13$ ,  $C_n^j = 1$  and using of two iterations.

The results of wavelet analysis and corresponding power spectrum for each pair of enhanced signals {P21, P31}, {P21, P51}, {P21, P72} and {P21, P12} are presented in Figs. 18, 19, 20 and 21, respectively.

In each figure, the energy density of the CWT (i.e.  $|W_\psi|^2$ ) of each signal, corresponding cross wavelets (that is  $|XW_\psi|$ ) and their spectral powers (that is  $P_W$  or  $P_{XW}$ ) are presented. In all figures, for the energy density  $|W_\psi|^2$  and the cross-wavelet  $|XW_\psi|$ , plotted ranges of energies are  $0.02Max[|W_\psi|^2] \leq |W_\psi|^2 \leq Max[|W_\psi|^2]$  and  $0.02Max[|XW_\psi|] \leq |XW_\psi| \leq Max[|XW_\psi|]$ , respectively.

Based on the cross-wavelet analysis and the corresponding power spectrum, the identified modal-like frequencies have peaks in the power spectral curves and are continuous through time in XWTs. To clarify detected frequencies, they are pointed by arrows in Figs. 18(e)-21(e)). The detected frequencies are:

- 1- For the pair {**P21, P31**} (Figs. 18(e,f)): 0.88, 0.92, 1.05, 1.085, 1.11, 1.21, 1.24, 1.29, 1.58, 1.64, 1.79, 1.835, 2.12, 2.16, and 2.28 Sec,
- 2- For the pair {**P21, P51**} (Figs. 19(e,f)): 0.88, 0.92, 1.05, 1.085, 1.24, 1.29, 1.58, 1.64, 1.79, 1.835, 2.12, 2.16, and 2.28 Sec,
- 3- For the pair {**P21, P72**} (Figs. 20(e,f)): 0.88, 0.92, 1.05, 1.085, 1.24, 1.29, 1.53, 1.54, 1.58, 1.64, 1.79, 1.835, 1.9, 1.97, 2.07, 2.12, 2.16, and 2.28 Sec,
- 4- For the pair {**P21, P12**} (Figs. 21(e,f)): 0.88, 0.92, 1.05, 1.085, 1.21, 1.24, 1.29, 1.58, 1.64, 1.695, 1.72, 1.79, 1.835, 2.12, and 2.16 Sec,

Since signals are not recorded simultaneously, common detected periods in all pairs are assumed to be possible modal periods. The common periods in all signal pairs are: 0.88, 0.92, 1.05, 1.085, 1.24, 1.29, 1.58, 1.64, 1.79, 1.835, 2.12, and 2.16 s. Also, the results show that due to the semi-symmetric shape of the structure, there are several pairs of nearly excited periods in the power spectrum (which may be two similar modes independently in the  $x$  and  $y$  directions).

Also, the main concrete tower was independently modeled by the linear finite element (FE) method using 3D continuum elements with linear shape functions [48]. The effects of damage, soil-structure interaction, concrete-steel interaction, elevators, and operating machinery and fans are not considered in the FE model. The modal frequencies obtained from the FE model are reported as: 0.1829, 0.1843, 0.20, 0.2138, 0.3139, 0.3232, 0.3954, 0.4118, 1.6004, and 1.9738 Sec [48].

According to the modal frequencies identified from the FE model, the possible reasons for the difference between the results from the ambient vibration test and the FE model could be:

- 1- The operation of mechanical systems and the existence of three active fans in the main tower.
- 2- There were four narrow steel towers on top of the main concrete tower. These steel towers are not considered in the FE model.
- 3- There is existence of (considerable) damage and cracks in different parts of the main tower, and the connection of the main tower with the neighboring structure. They were not considered in the FE model,
- 4- Four narrow and long steel towers are above the main structure. However, they are not simulated in the FEM.

## 9. Conclusion and future study

In this work, introducing the iterative enhancing approach based on wavelet packet transform is the main goal. As the authors know, this is the first time that wavelet packet based iterative denoising is used for ambient vibration tests. Also, both the one-step and the iterative denoising methods (based on MRA) have been investigated to improve the signals with a high level of noise recorded from ambient vibration tests. In this study with a benchmark involving high level of noise, the robustness of the iterative denoising method is studied; the result is compared with the common one-step denoising method with different thresholds. The results of the one-step denoising methods confirm that:

- 1) Outputs still need considerable improvement, due to small values of PSNR (Table 3 and Fig. 15),
- 2) From different thresholding methods, different results can be obtained,

For the wavelet-packet based iterative denoising method for high-level of noise in data, it may be possible to conclude:

- 1) The wavelet-packet based iterative denoising approach can enhance the signals (see captured noise in Fig. 16 and corresponding energy density of noise in Fig. 17),
- 2) This method can effectively detect random local data. This confirms the importance of using iterative denoising approaches for data enhancement (noise energy in Fig. 17).
- 3) Noise in the signal cannot completely be removed even by the iterative method (see remaining localized features in Fig. 19).

After enhancement of high-level noisy signals (recorded from ambient vibration tests) by the iterative denoising method, it has been tried to identify the excited frequencies by using the continuous cross-wavelet analyses and the corresponding spectral powers. In the continuous wavelet transform, Morlet complex wavelets are used to detect both instantaneous frequencies and corresponding excitation patterns in the time-frequency representation. The excited frequency is recognized as a physical phenomenon with continuous excitation over time in the time-frequency representation. Regarding their spectral powers, also, these modal frequencies have local concentrations with considerable powers around modal frequencies (or corresponding scales). By cross-analyzing of the pairs of enhanced signals, the results confirm:

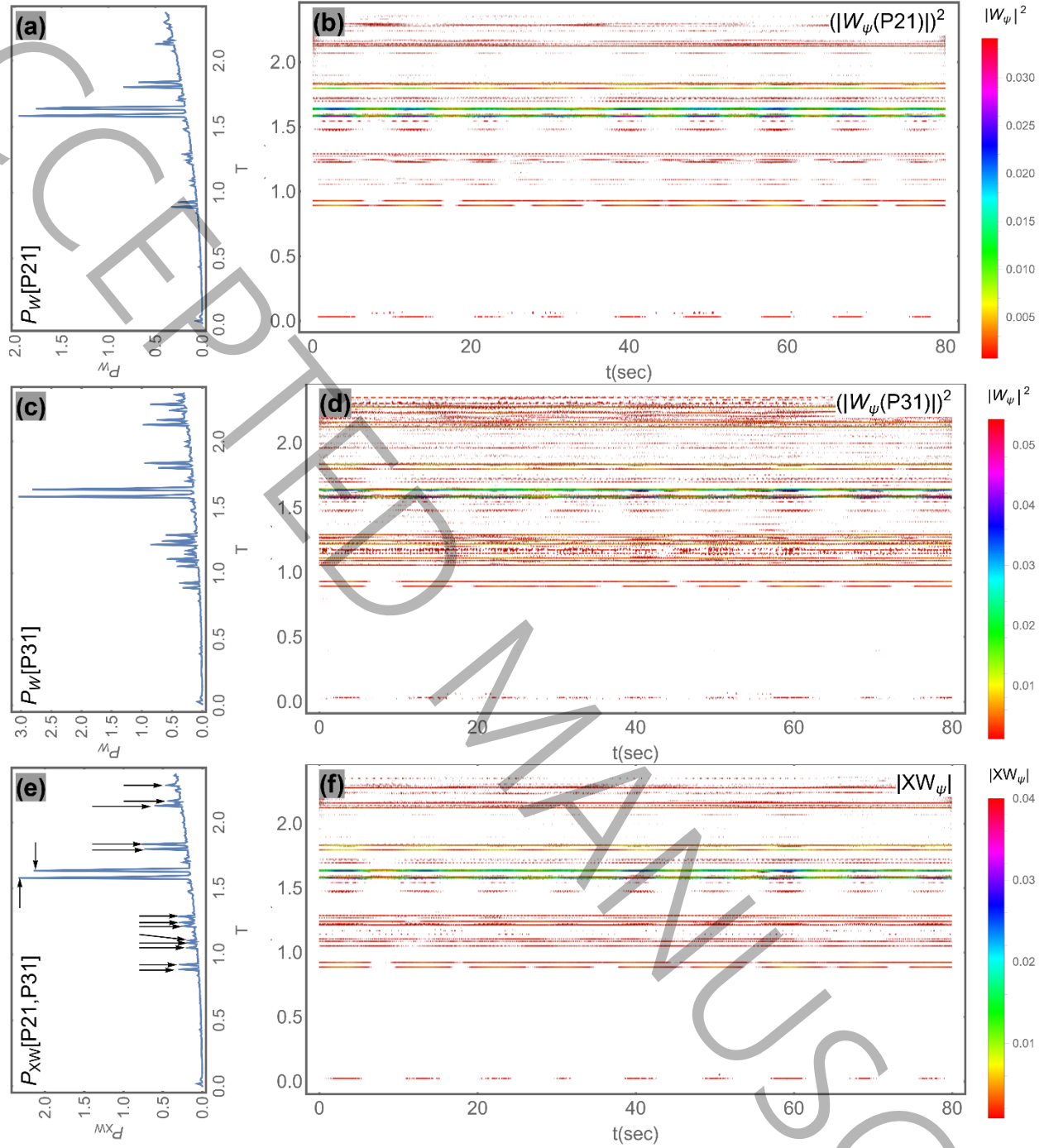


**Fig.18: Powers and energies of wavelet transforms of denoised signals P21 and P31, and corresponding XWT and spectral power of XWT; a) The spectral power of denoised P21 ; b) The density of energy for the denoised P21,  $|W_\psi(P21)|^2$ ; c) The spectral power of denoised P31 d) The density of energy for the denoised P31,  $|W_\psi(P31)|^2$ ; e) The spectral power of XWT for the denoised data P21 and P31; f) The density of  $|XW_\psi|$  for the denoised data P21 and P31 . In these figures, plotted graphs are for the range  $0.02\text{Max}[|W_\psi|^2] \leq |W_\psi|^2 \leq \text{Max}[|W_\psi|^2]$  or  $0.02\text{Max}[|XW_\psi|] \leq |XW_\psi| \leq \text{Max}[|XW_\psi|]$ .**

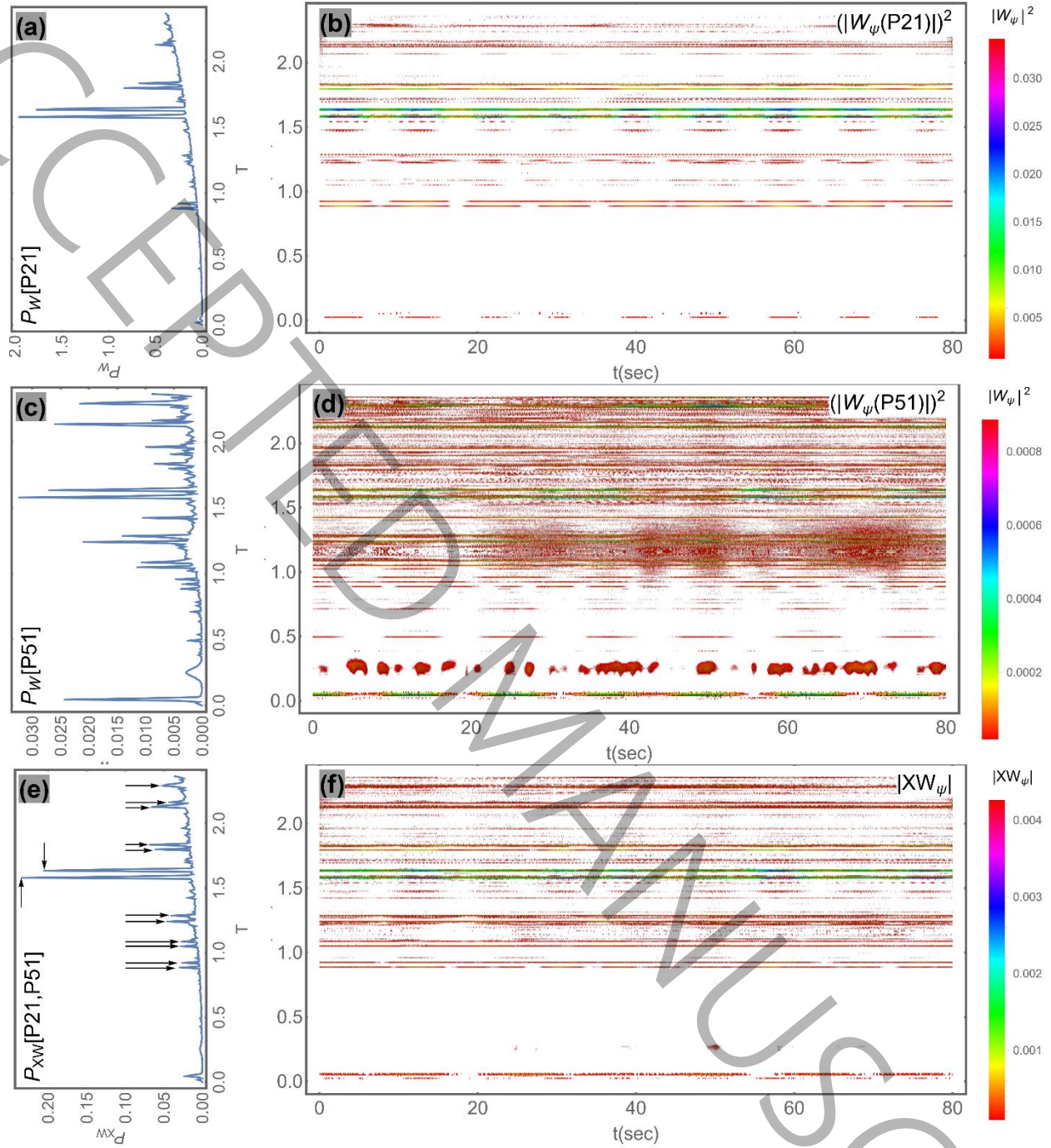


Fig. 19: Powers and energies of wavelet transforms of denoised signals P21 and P51 and corresponding XWT and spectral power of XWT; a) The spectral power of denoised P21 ; b) The density of energy for the denoised P21,  $|W_\psi(P21)|^2$ ; c) The spectral power of denoised P51 d) The density of energy for the denoised P51,  $|W_\psi(P51)|^2$ ; e) The spectral power of XWT for the denoised data P21 and P51; f) The density of  $|XW_\psi|$  for the denoised data P21 and P51. In these figures, plotted graphs are for the range  $0.02\text{Max}[|W_\psi|^2] \leq |W_\psi|^2 \leq \text{Max}[|W_\psi|^2]$  or  $0.02\text{Max}[|XW_\psi|] \leq |XW_\psi| \leq \text{Max}[|XW_\psi|]$ .

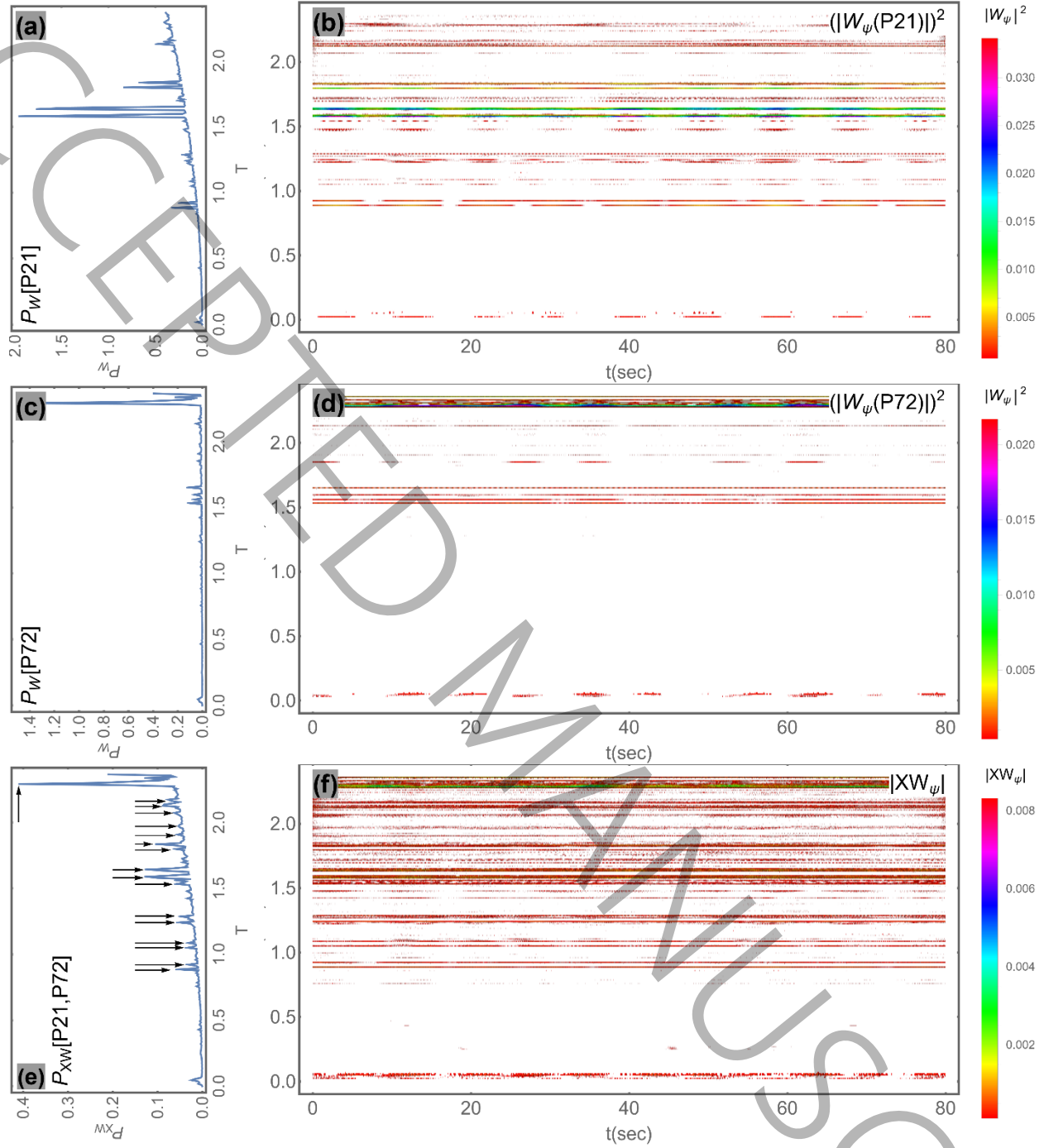
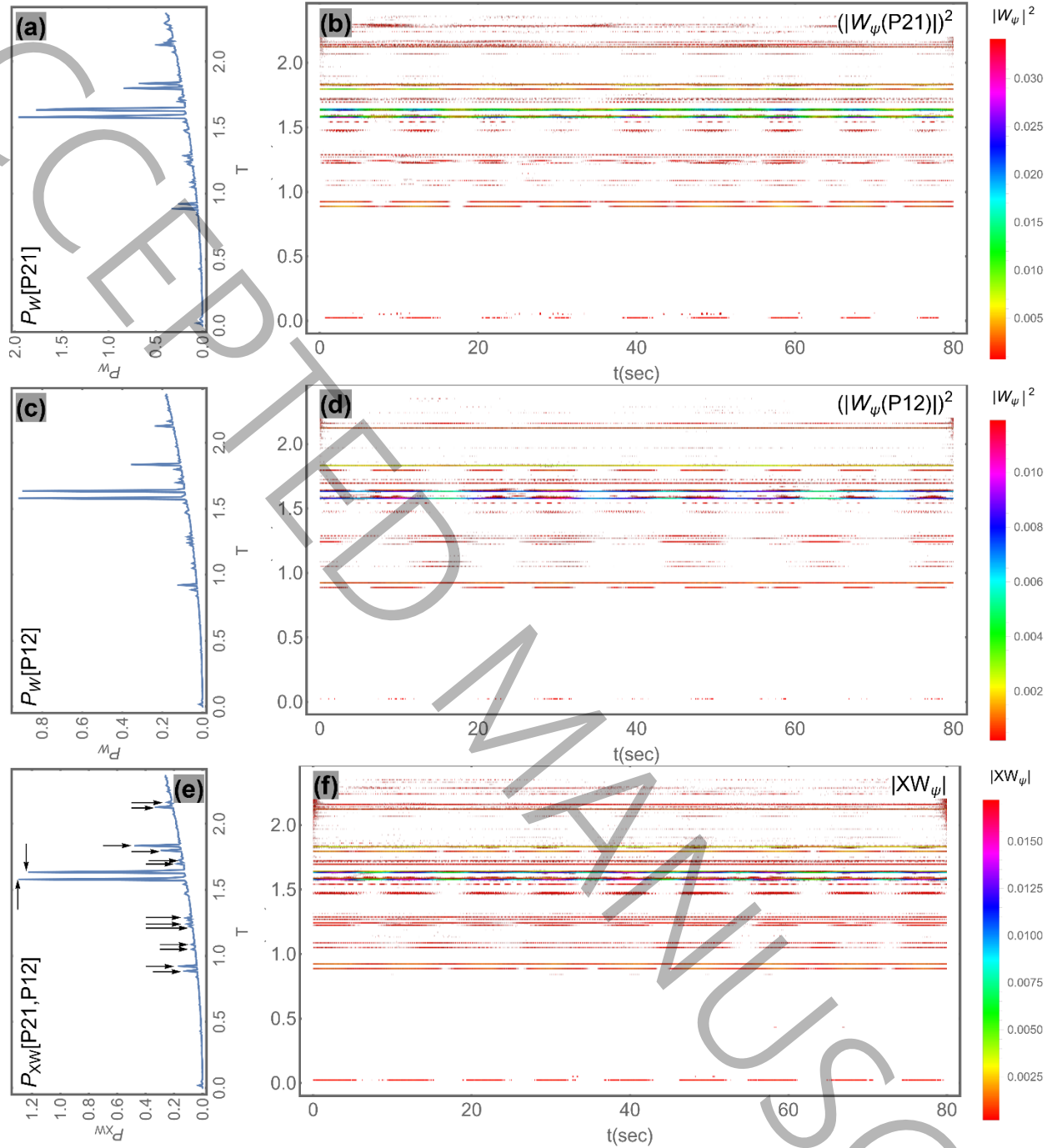


Fig. 20: Powers and energies of wavelet transforms of denoised signals P21 and P72 and corresponding XWT and spectral power of XWT; a) The spectral power of denoised P21 ; b) The density of energy for the denoised P21,  $|W_\psi(P21)|^2$ ; c) The spectral power of denoised P72 d) The density of energy for the denoised P72,  $|W_\psi(P72)|^2$ ; e) The spectral power of XWT for the denoised data P21 and P72; f) The density of  $|XW_\psi|$  for the denoised data P21 and P72. In these figures, plotted graphs are for the range  $0.02\text{Max}[|W_\psi|^2] \leq |W_\psi|^2 \leq \text{Max}[|W_\psi|^2]$  or  $0.02\text{Max}[|XW_\psi|] \leq |XW_\psi| \leq \text{Max}[|XW_\psi|]$ .



**Fig. 21: Powers and energies of wavelet transforms of denoised signals P21 and P12, and corresponding XWT and spectral power of XWT; a) The spectral power of denoised P21 ; b) The density of energy for the denoised P21,  $|W_\psi(P21)|^2$ ; c) The spectral power of denoised P12 d) The density of energy for the denoised P12,  $|W_\psi(P12)|^2$ ; e) The spectral power of XWT for the denoised data P21 and P12; f) The density of  $|XW_\psi|$  for the denoised data P21 and P12. In these figures, plotted graphs are for the range  $0.02\text{Max}[|W_\psi|^2] \leq |W_\psi|^2 \leq \text{Max}[|W_\psi|^2]$  or  $0.02\text{Max}[|XW_\psi|] \leq |XW_\psi| \leq \text{Max}[|XW_\psi|]$ .**

- 1) Cross-wavelet analysis improves the time-frequency representation for identifying excited frequencies (e.g., Fig. 19),
- 2) Despite the improved time-frequency representation of cross wavelets, this transformation may also be insufficient because of existence of several continuous frequencies in its time-frequency representation. As it is not clear whether these frequencies are modal frequencies or not (Figs. 18-20),
- 3) However, the spectral power of the wavelet transform could be useful for detection and capturing the frequency of significant energies (as physical phenomena),
- 4) Due to the nearly symmetrical plane of the structure, the detected modal frequencies are close to each other (see Fig. 2) (however for the torsional modal frequencies, it is not the case),
- 5) Cross wavelet analysis could reduce the effects of stochastic phenomena such as noise, as they do not have coherence with each other (see Fig. 19).

At the end of this study, the detected frequencies are compared with the frequencies captured from the 3D FE model. They have good agreements with each other. However, there are frequencies that are not seen in the FE model, which could be due to the following reasons:

- 1- The operation of mechanical systems and the existence of three active fans in the main tower,
- 2- There were four narrow steel towers on top of the main concrete tower. These steel towers are not considered in the FE model,
- 3- Existence of damage and cracks in different parts of the main tower, which is not considered in the FE model.

Finally, it should be noted that the common discrete wavelet (packet) based one-step denoising with different threshold may lead to over- or under-smoothing results for signals with high level of noise (as presented in Fig. 4 and Table 1). Hence, for such data, the wavelet-based iterative approach could be promising along with other common methods. Also, the finite element model in [48] was not based on the model-updating approach to achieve more accurate model: it was an initial model based on initial assumptions which should be updated. Hence, model updating would be recommended.

In conclusion, for civil engineering applications, vibration responses are complex, displaying variations in space and time. The responses often contain nonlinearity and uncertainties not considered during data collection. These responses can also be polluted by various sources, affecting numerical simulations and damage identification processes. A significant challenge is how to effectively remove noise from the collected data to achieve reliable damage indicators that are insensitive to noise and environmental factors. Hence, proper denoising, damage detection and numerical simulations are still active research areas [57].

For future study, wavelet based denoising approach is a powerful tool; some of recent studies can be mentioned as: (1) Using of the iterative denoising method based on the lifting wavelet transform [58], (2) Using the iterative algorithm enhanced by using the statistical process control [59], (3) Selection of optimum wavelet family for denoising [60], (4) Improving thresholding approach for signal denoising using for structural health monitoring [61], (5) Combining of other type of filtering with wavelet thresholding to enhance denoising [62]. Also, for a comparative study of wavelet transforms for the health monitoring, one can see [63].

## References

1. Y. Tamura, Damping in buildings and estimation techniques, In: Y. Tamura, A. Kareem, editors. *Advanced Structural Wind Engineering*: Springer, (2013) 347-76.
2. L. Carassale, F. Percivale, editors. *POD-based modal identification of wind-excited structures*. Proceedings of the Twelfth International Conference on Wind Engineering, Cairns, Australia (2007).
3. T.-H. Le, Y. Tamura, editors. *Modal identification of ambient vibration structure using frequency domain decomposition and wavelet transform*, Proceedings of the 7th Asia-Pacific conference on wind engineering, Taipei, Taiwan (2009).
4. J. Lardies, S. Gouttebroze, Identification of modal parameters using the wavelet transform, *International Journal of Mechanical Sciences*, 44(11) (2002) 2263-83.
5. X. He, B. Moaveni, J.P. Conte, A. Elgamal, S. F. Masri, Modal identification study of Vincent Thomas bridge using simulated wind-induced ambient vibration data, *Computer-Aided Civil and Infrastructure Engineering*, 23(5) (2008) 373-88.
6. X. H. He, X. G. Hua, Z. Q. Chen, F. L. Huang, EMD-based random decrement technique for modal parameter identification of an existing railway bridge, *Engineering Structures*, 33(4) (2011) 1348-56.
7. C. S. Huang, S. L. Hung, C. I. Lin, W. C. Su, A wavelet-based approach to identifying structural modal parameters from seismic response and free vibration data, *Computer-Aided Civil and Infrastructure Engineering*, 20(6) (2005) 408-23.
8. K. K. Wijesundara, C. Negulescu, E. Foerster, D. Monfort Climent, Estimation of modal properties of structures through ambient excitation measurements using continuous wavelet transform, *Engineering Structures* (2012).
9. T. Kijewski, A. Kareem, Wavelet transforms for system identification in civil engineering, *Computer-Aided Civil and Infrastructure Engineering*, 18(5) (2003) 339-55.
10. J. Lin, L. Qu, Feature extraction based on Morlet wavelet and its application for mechanical fault diagnosis. *Journal of Sound and Vibration*, 234(1) (2000) 135-48.
11. K. F. Al-Raheem, A. Roy, K. P. Ramachandran, D. K. Harrison, S. Grainger, Rolling element bearing faults diagnosis based on autocorrelation of optimized: wavelet de-noising technique, *International Journal of Advanced Manufacturing Technology*, 40(3-4) (2009) 393-402.
12. B. Yan, A. Miyamoto, E. Brühwiler, Wavelet transform-based modal parameter identification considering uncertainty, *Journal of Sound and Vibration*, 291(1) (2006) 285-301.
13. X. Jiang, H. Adeli, Pseudospectra, MUSIC, and dynamic wavelet neural network for damage detection of highrise buildings, *International Journal for Numerical Methods in Engineering*, 71(5) (2007) 606-29.
14. R. A. Osornio-Rios, J. P. Amezcua-Sanchez, R. J. Romero-Troncoso, A. Garcia-Perez, MUSIC-ANN analysis for locating structural damages in a truss-type structure by means of vibrations, *Computer-Aided Civil and Infrastructure Engineering* 27(9) (2012) 687-98.
15. M. Meo, G. Zumpano, X. Meng, E. Cosser, G. Roberts, A. Dodson, Measurements of dynamic properties of a medium span suspension bridge by using the wavelet transforms, *Mechanical Systems and Signal Processing*, 20(5) (2006) 1112-33.
16. N. Kang, H. Kim, S. Choi, S. Jo, J. S. Hwang, E. Yu, Performance evaluation of TMD under typhoon using system identification and inverse wind load estimation, *Computer-Aided Civil and Infrastructure Engineering*, 27(6) (2012) 455-73.

17. C. S. Huang, W. C. Su, Identification of modal parameters of a time invariant linear system by continuous wavelet transformation, *Mechanical Systems and Signal Processing*, 21(4) (2007) 1642-64.
18. B. Yan, A. Miyamoto. A comparative study of modal parameter identification based on wavelet and Hilbert–Huang transforms, *Computer-Aided Civil and Infrastructure Engineering*, 21(1) (2006) 9-23.
19. W. C. Su, C. S. Huang, C. H. Chen, C. Y. Liu, H. C. Huang, Q. T. Le, Identifying the modal parameters of a structure from ambient vibration data via the stationary wavelet packet, *Computer-Aided Civil and Infrastructure Engineering*, 29(10) (2014) 738-57.
20. W. C. Su, C. Y. Liu, Huang CS. Identification of instantaneous modal parameter of time-varying systems via a wavelet-based approach and its application, *Computer-Aided Civil and Infrastructure Engineering*, 29(4) (2014) 279-98.
21. S.-L. Chen, J.-J. Liu, H.-C. Lai, Wavelet analysis for identification of damping ratios and natural frequencies, *Journal of Sound and Vibration*, 323(1) (2009) 130-47.
22. R. X. Gao, R. Yan, *Wavelets: Theory and Applications for Manufacturing: Springer Science & Business Media* (2010).
23. N. E. Huang, Introduction to the Hilbert Huang transform and its related mathematical problems, In: N. E. Huang, S. S. P. Shen, editors. *Hilbert-Huang Transform and its Applications: World Scientific*, (2011) p. 1-26.
24. A. Teolis, *Computational Signal Processing with Wavelets: Springer Science & Business Media* (2012).
25. M. Misiti, Y. Misiti, G. Oppenheim, J.-M. Poggi, *Wavelets and Their Applications: John Wiley & Sons*, 2013.
26. S. Mallat, *A Wavelet Tour of Signal Processing, (Wavelet Analysis & Its Applications): Academic Press*, 1999.
27. P. Van Fleet, *Discrete Wavelet Transformations: An Elementary Approach with Applications: John Wiley & Sons*, 2008.
28. M. Jansen, *Noise Reduction by Wavelet Thresholding: Springer Science & Business Media* (2012).
29. K. P. Soman, *Insight into Wavelets: From Theory to Practice: PHI Learning Pvt. Ltd.* (2010).
30. R. R. Coifman, M. V. Wickerhauser, Adapted waveform “de-Noising” for medical signals and images, *IEEE Engineering in Medicine and Biology Magazine*, 14(5) (1995) 578-86.
31. R. R. Coifman, M. V. Wickerhauser, Experiments with adapted wavelet de-noising for medical signals and images. In: Akay M, editor. *Time Frequency and Wavelets in Biomedical Signal Processing: IEEE press series in Biomedical Engineering* (1998).
32. L. J. Hadjileontiadis, S. M. Panas, Separation of discontinuous adventitious sounds from vesicular sounds using a wavelet-based filter, *IEEE Transactions on Biomedical Engineering*, 44(12) (1997) 1269-81.
33. L. J. Hadjileontiadis, C. N. Liatsos, C. C. Mavrogiannis, T. A. Rokkas, S. M. Panas, Enhancement of bowel sounds by wavelet-based filtering, *IEEE Transactions on Biomedical Engineering*, 47(7) (2000) 876-86.
34. R. Ranta, C. Heinrich, V. Louis-Dorr, D. Wolf, Interpretation and improvement of an iterative wavelet-based denoising method. *IEEE Signal Processing Letters*, 10(8) (2003) 239-41.
35. R. Ranta, V. Louis-Dorr, C. Heinrich, D. Wolf, Iterative wavelet-based denoising methods and robust outlier detection. *IEEE Signal Processing Letters*, 12(8) (2005) 557-60.
36. J.-L. Starck, A. Bijaoui. Filtering and deconvolution by the wavelet transform, *Signal Process*, 35(3) (1994) 195-211.
37. A. Grinsted, J. C. Moore, S. Jevrejeva, Application of the cross wavelet transform and wavelet coherence to geophysical time series, *Nonlinear Processes Geophys*, 11(5/6) (2004) 561-6.
38. W. J. Staszewski, Identification of damping in MDOF systems using time-scale decomposition, *Journal of Sound and Vibration*, 203(2) (1997) 283-305.
39. J. Guo, G. Wei, X. Li, D. Jin, F. Liu, Modal identification of structures with closely spaced modes based on improved empirical wavelet transform, *Journal of Vibration Engineering & Technologies*, 10(7) (2022) 2625-2640.
40. Zh. Bai, J. Wei, K. Chen, Kaiyan Wang, ICEEMDAN and improved wavelet threshold for vibration signal joint denoising in OPAX, *Journal of Mechanical Science and Technology*, 38 (2024) 1-11.
41. K. C. Raath, K. B. Ensor, A. Crivello, D. W. Scott, Denoising non-stationary signals via dynamic multivariate complex wavelet thresholding, *Entropy* 25(11) (2023) 1546.
42. A. Silik, M. Noori, W.A. Altabay, J. Dang, R. Ghiasi, A new denoising technique via wavelet analysis of structural vibration response for structural health monitoring applications, *Lifelines* (2022) 691-706.
43. A. Silik, M. Noori, Z. Wu, W.A. Altabay, J. Dang, N. S. Farhan, Wavelet-based vibration denoising for structural health monitoring, *Urban Lifeline*, 2024 2(1), 1-14.
44. Q. Liao, Z. Sheng, P. Guo, Research on the Wavelet Denoising Algorithm for Thorpe Analysis Based on the Radiosonde Data, *Remote Sensing*, 17(1) 2025,114-126.

45. X. An, C. Li, F. Zhang, Application of adaptive local iterative filtering and approximate entropy to vibration signal denoising of hydropower unit, *Journal of Vibroengineering*, 2016 18(7), 4299-4311.
46. H. Yousefi, A. Taghavi Kani, I. Mahmoudzadeh Kani, S. Mohammadi, Wavelet-based iterative data enhancement for implementation in purification of modal frequency for extremely noisy ambient vibration tests in Shiraz-Iran, *Frontiers of Structural and Civil Engineering*, 14 (2020) 446-472.
47. H. Yousefi, S. S. Ghorashi, T. Rabczuk, Directly simulation of second order hyperbolic systems in second order form via the regularization concept, *Communications in Computational Physics*, 20(1) (2016) 86-135.
48. J. Samadi, Seismic Behavior of Structure-Equipment in a Petrochemical Complex to Evaluate Vulnerability Assessment: a Case Study, University of Tehran (2010).
49. Shin, K. and Hammond, J., *Fundamentals of Signal Processing for Sound and Vibration Engineers*, (2008) John Wiley & Sons.
50. S. Mallat, *A Wavelet Tour of Signal Processing, Third Edition: The Sparse Way*, Academic Press, Inc., 2008.
51. P. Van Fleet, *Discrete Wavelet Transformations: An Elementary Approach with Applications*, John Wiley & Sons, (2019).
52. M. Jansen, *Noise Reduction by Wavelet Thresholding*, Springer Science & Business Media, 2001.
53. D.L. Donoho, J.M. Johnstone, Ideal spatial adaptation by wavelet shrinkage. *Biometrika*, 81 (1994) 425-455.
54. C.M. Stein, Estimation of the mean of a multivariate normal distribution, *Annals of Statistics*, (1981) 1135-1151.
55. K. M. Jeevan, S. Krishnakumar, An algorithm for wavelet thresholding based image denoising by representing images in hexagonal lattice, *Journal of Applied Research and Technology*, 16(2) (2018) 103-114.
56. [Wavelet denoising — skimage 0.24.0 documentation.](#)
57. A. Mansi, L. Dunai, M. Cao, Wavelet-based denoising of structural health monitoring strain measurements, *Measurement: Sensors*, 42 (2025) 101974.
58. S. A. Malik, S. A. Parah, H. Aljuaid, B. A. Malik, An iterative filtering based ECG denoising using lifting wavelet transform technique, *Electronics*, 12(2) (2023) 387.
59. F. M. Bayer, A. J. Kozakevicius, R. J. Cintra. An iterative wavelet threshold for signal denoising, *Signal Processing* 162 (2019) 10-20.
60. A. Silik, M. Noori, W. A. Altabay, J. Dang, R. Ghiasi, and Zh. Wu, Optimum wavelet selection for nonparametric analysis toward structural health monitoring for processing big data from sensor network: A comparative study, *Structural Health Monitoring*, 21(3) (2022) 803-825.
61. X. Jiang, Q. Lang, Q. Jing, H. Wang, J. Chen, and Q. Ai, An improved wavelet threshold denoising method for health monitoring data: A case study of the Hong Kong-Zhuhai-Macao Bridge immersed tunnel, *Applied Sciences*, 12(13) (2022) 6743.
62. G. Jia, J. Yang, and H. Liang, A Combined Denoising Method of Adaptive VMD and Wavelet Threshold for Gear Health Monitoring, *Structural Durability & Health Monitoring* 19(4) (2025).
63. A. Silik, M. Noori, W. A. Altabay, R. Ghiasi, and Zh. Wu, Comparative analysis of wavelet transform for time-frequency analysis and transient localization in structural health monitoring, *Structural Durability & Health Monitoring*, 15(1) (2021) 1.